# Charge Separation and Surface Reconstruction:

## A $Mn^{2+}$ Doping of $TiO_2$ Nanoparticles Study

***Dr Zoran Šaponjić***

***Vinca Institute of Nuclear Sciences***

Overview:

- definition of nanomaterials;
- properties and applications of titanium dioxide ($TiO_2$) nanocrystals;
- synchrotron (X-ray) radiation based analytical methods;
- electron paramagnetic resonance
- $Mn^{2+}$ doped $TiO_2$ nanoparticles.

# Nano is big business
## (Prof. Marc Ratner)

American National Science Foundation (NSF) predicts that nano-related goods and services could be a $1 trillion market by 2015, making it not only one of the fastest-growing industries in history but also larger than the combined telecommunications and information technology industries at the beginning of the technology boom in 1998.

Nanoscale science and engineering here refer to the **fundamental understanding and resulting technological** advances arising **from the exploitation of new physical, chemical and biological properties of systems** that are **intermediate in size, between isolated atoms and molecules and bulk materials**, where the transitional properties between the two limits can be controlled.

The cross section for elastic scattering from a 50 nm gold nanocrystals is million-fold larger than the cross section for absorption or emission of electromagnetic radiation from any molecule or even quantum dot chromophore.

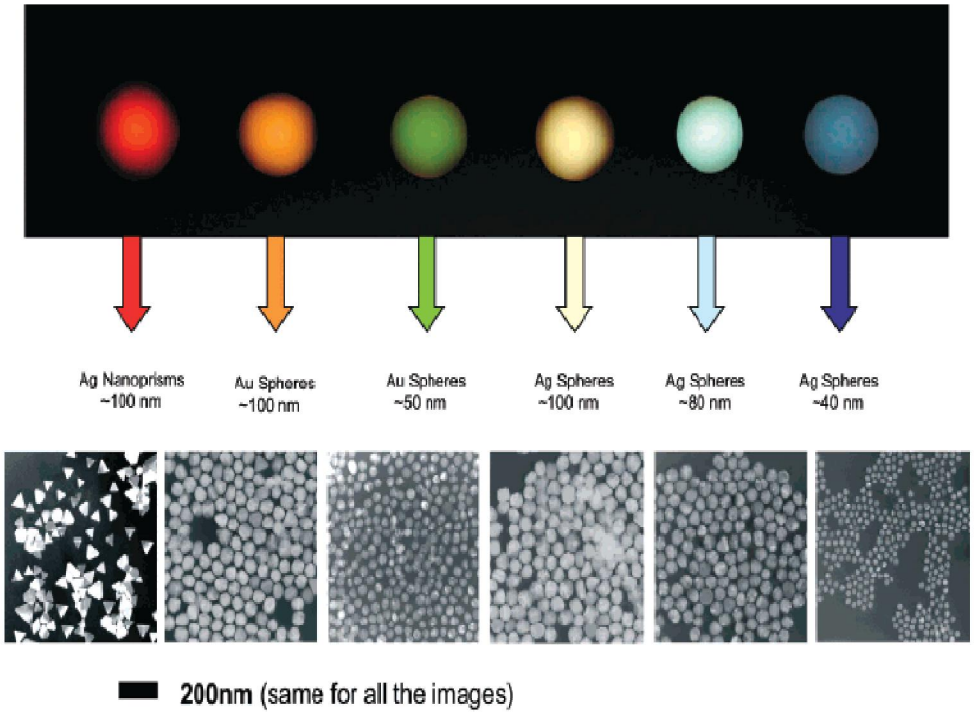


**Figure 1.** Sizes, shapes, and compositions of metal nanoparticles can be systematically varied to produce materials with distinct light-scattering properties.

In a metallic nanoparticles, incident light can couple to the plasmon excitation of the metal which involves the light induced motion of the valence electrons.

-**quantum dots (QDs)**, are semiconductor composed of:

periodic groups of **II–VI elements (e.g., CdS, CdSe, CdTe, ZnS, ZnSe) or III–V elements (e.g., InP, GaAs)**

A (Wannier) exciton can be defined as the bound state of an electron-hole pair, due to a Coulomb interaction between the charge carriers.
The distance between the electron and the hole is the Bohr radius of the exciton, $a_B$:

$$a_B = \frac{4\pi\varepsilon_0\varepsilon_\infty \hbar^2}{m_0 e^2}\left(\frac{1}{m_e^*} + \frac{1}{m_h^*}\right)$$

$m_e^*$ and $m_h^*$ are the effective electron and hole masses, respectively,
$\varepsilon_\infty$ is the high-frequency relative dielectric constant of the medium.

The resulting Bohr radius is much larger than that of a hydrogen atom, since the effective masses are considerably smaller than the mass of the electron at rest, $m_0$, and $\varepsilon\infty$ is considerably larger than 1.

Values for $a_B$ for the common semiconductors are in the range 10-100 Å (1-10 nm)

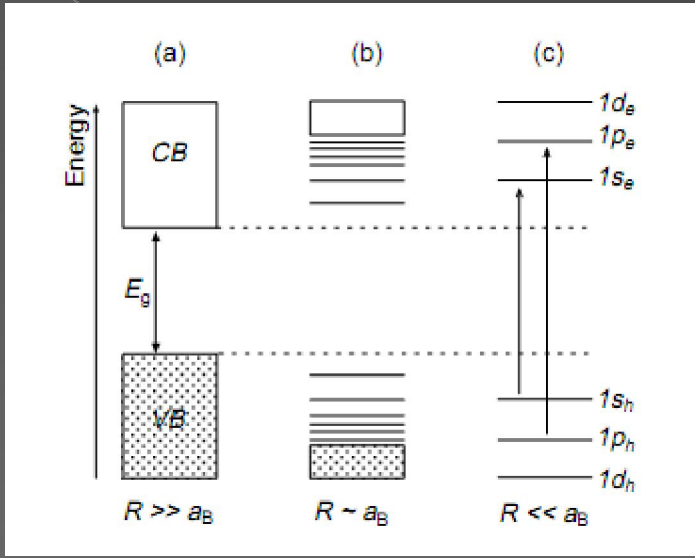


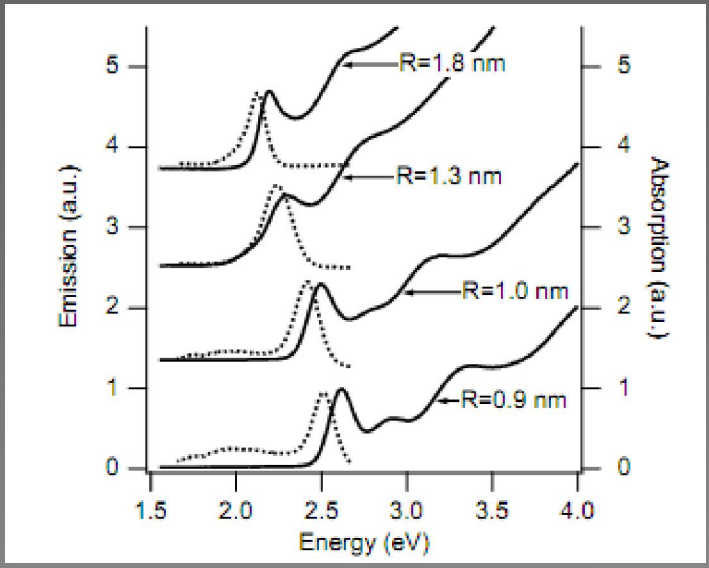


The effect of size on the electronic structure of a semiconductor crystal for three different size-ranges:

(a) a macrocrystalline semiconductor ($R >> a_B$) with continuous energy bands;
the filled valence band (VB) and empty conduction band (CB) and the bandgap energy ($E_g$).

(b) semiconductor nanocrystal with a weak size-quantization ($R \sim a_B$).

(c) highly quantised dot ($R << a_B$) with discrete atomic-like energy levels and optical transitions.

Absorption (solid lines) and emission (dotted lines) spectra of colloidal CdSe quantum dots, showing that the absorption edge shifts towards higher energies with respect to bulk CdSe (1.84 eV) and that discrete energy bands become more pronounced as the particle size decreases.

robust **fluorescence** emitters with **size-dependent emission wavelengths from UV to IR**.

**~2 nm** nanocrystals made of **CdSe** emit in the range between **495 to 515 nm**,

larger **~5nm CdSe** nanocrystals emit between **605 and 630 nm**.

-**extreme brightness** and **resistance to photobleaching** enables the use of very low laser intensities over extended time periods

-especially **useful for live-cell imaging**,

-the intense brightness is helpful for **single-particle detection** and an increasing number of biomedical assays.

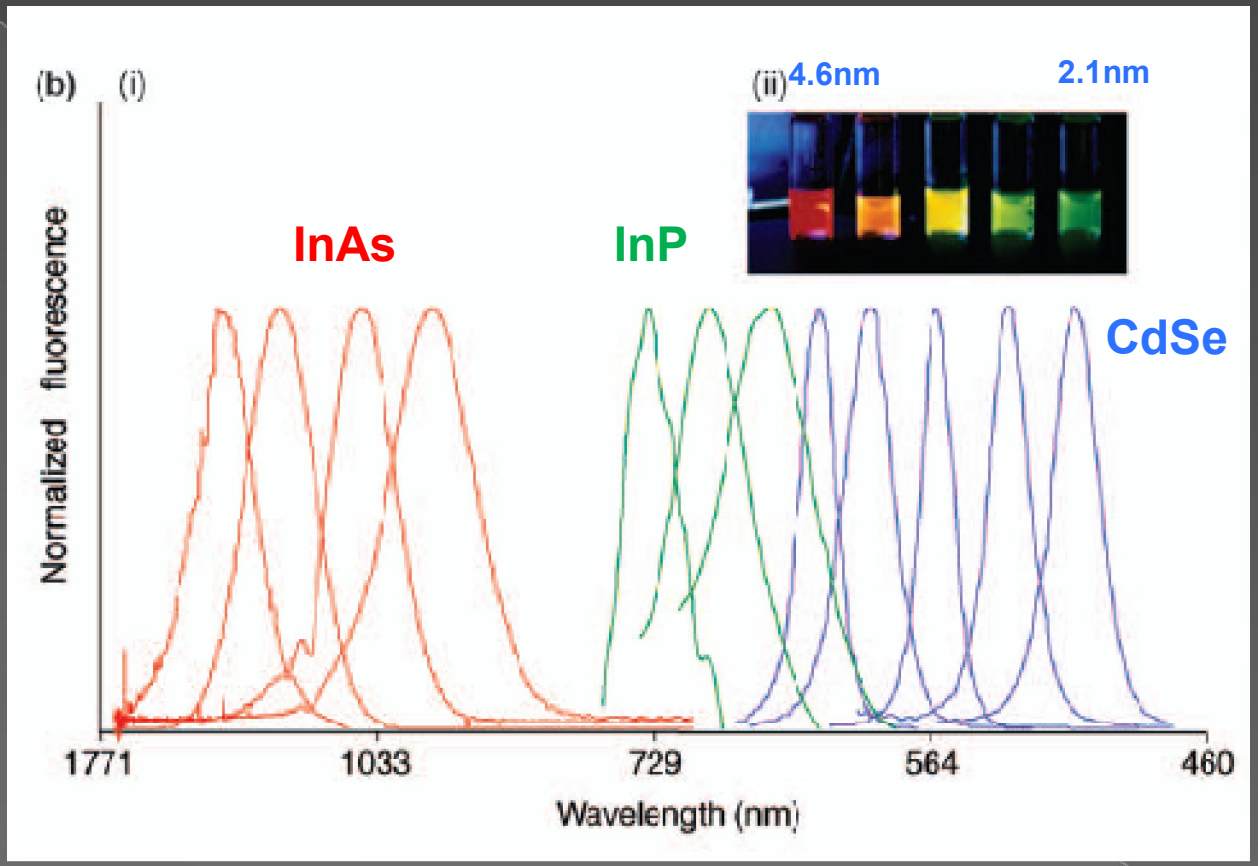


A true-color image of a series of silica-coated core (CdSe)-shell (ZnS or CdS) nanocrystal probes in aqueous buffer all illuminated simultaneously with a ultraviolet lamp.

- Size- and material- dependent emission spectra of several surfactant-coated QDs in a variety of sizes:

-the blue series represents different sizes of **CdSe QDs** with diameters of **2.1, 2.4, 3.1, 3.6 and 4.6 nm** (from right to left).

-the green series represents **InP (indium phosphide) QDs** with diameters of **3.0, 3.5, and 4.6 nm**.

-the red series represents **InAs (indium arsenide) QDs** with diameters of **2.8, 3.6, 4.6, and 6.0 nm** (arbitrary units on y-axis).

# $TiO_2$

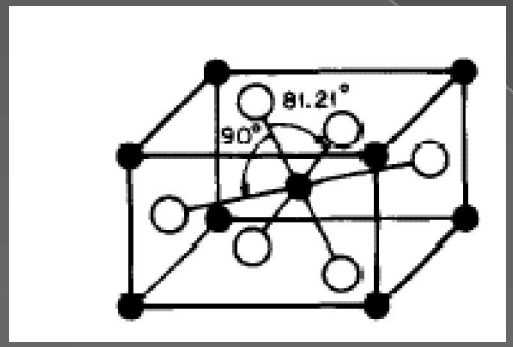


Rutile $TiO_2$
(tetragonal)

$d_{Ti-O}$ = 1.949 Å
$d_{Ti-Ti}$ = 3.57 Å

Eg= 3.0 eV
ρ = 4.250 g/cm³
$\Delta G_f$= -212.6 kcal/mol

● Titania

O Oxygen

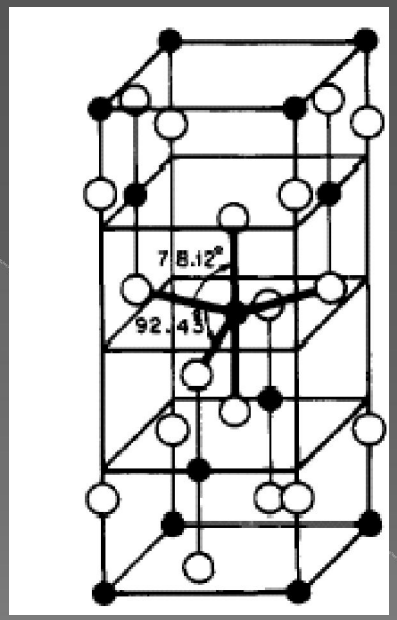


Anatase $TiO_2$
(tetragonal)

$d_{Ti-O}$ = 1.939 Å
$d_{Ti-Ti}$ = 3.79 Å

Eg= 3.2 eV
ρ = 3.894 g/cm³
$\Delta G_f$= -211.4 kcal/mol

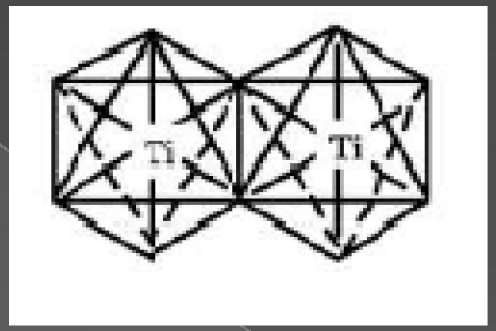


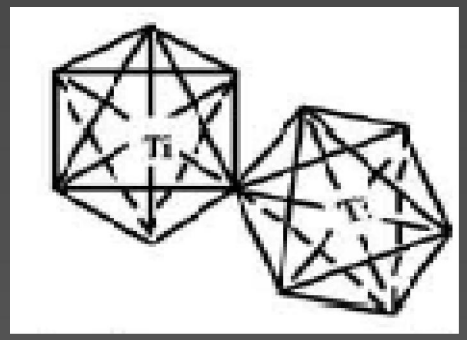


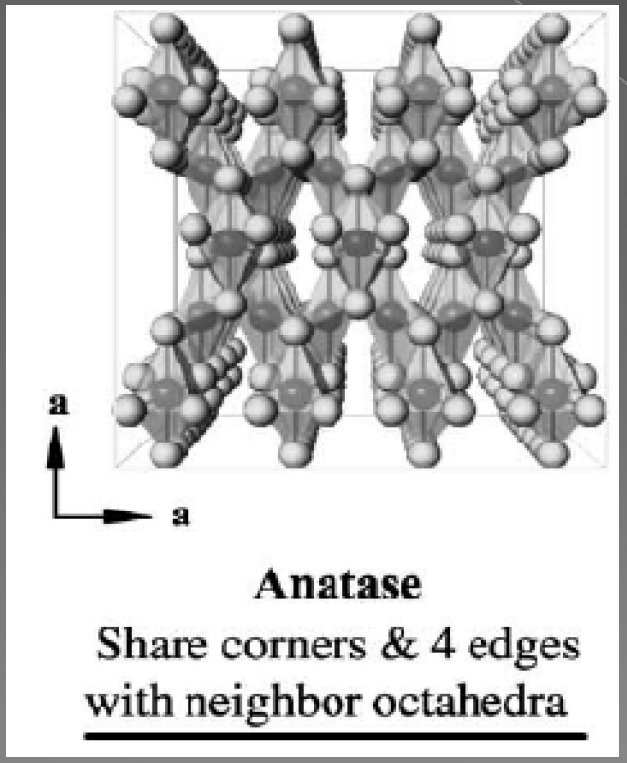


**Anatase**

Share corners & 4 edges with neighbor octahedra

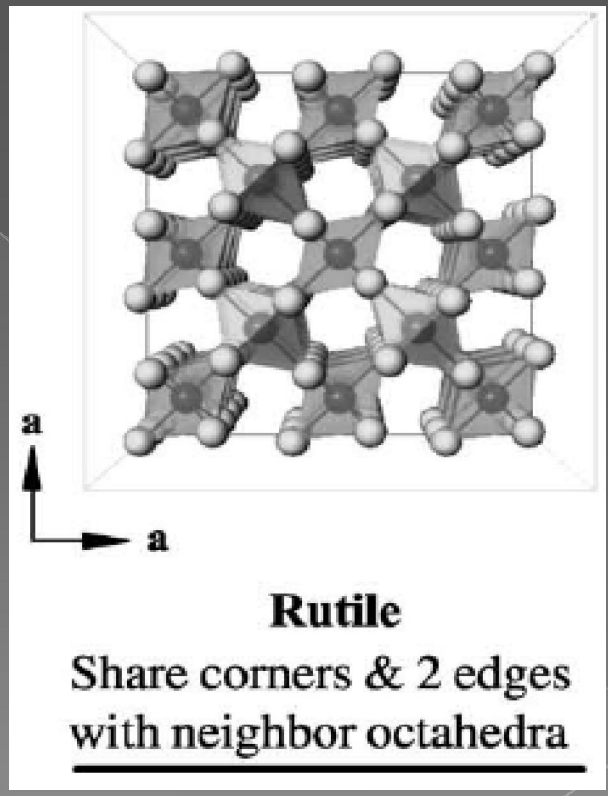


**Rutile**

Share corners & 2 edges with neighbor octahedra

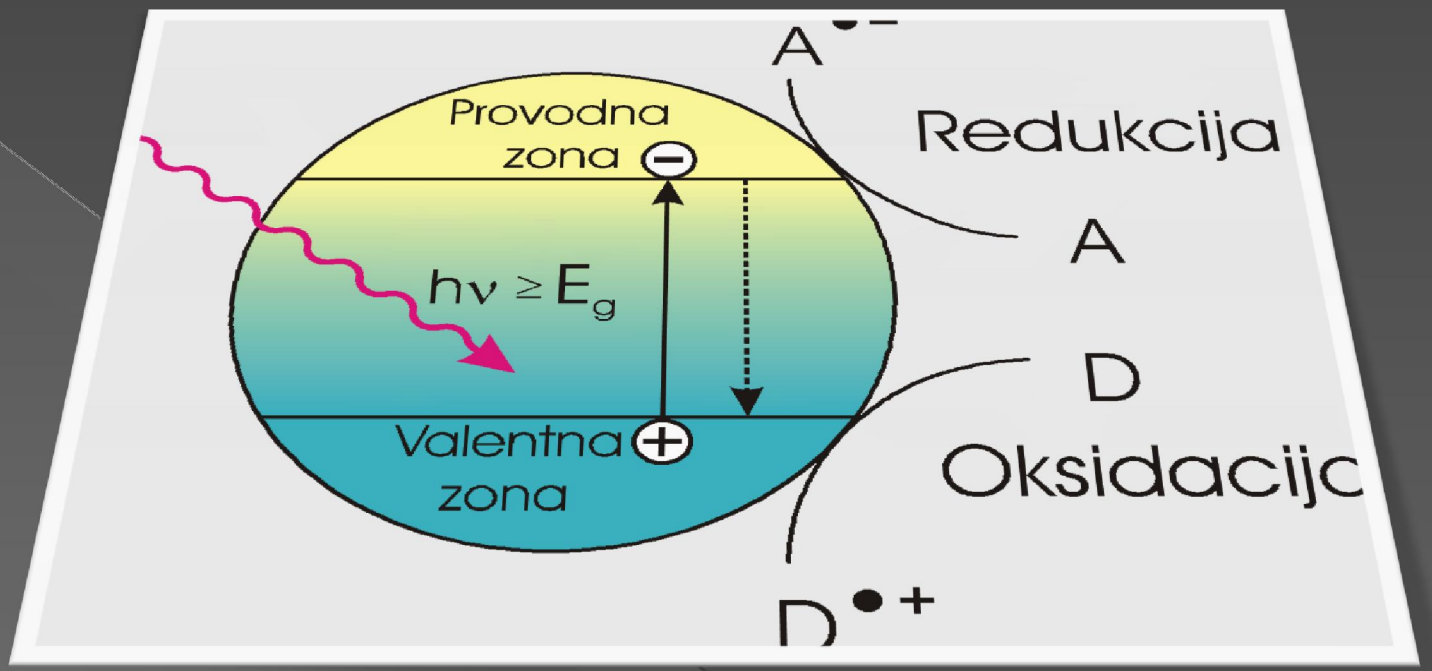


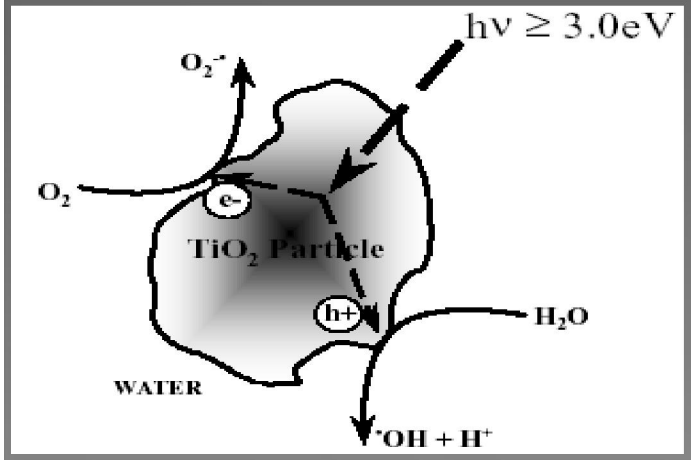


$$TiO_2 \xrightarrow{h\nu} e^- + h^+ + TiO_2$$

$$e^- + h^+ + TiO_2 \longrightarrow TiO_2 + heat\ and/or\ h\nu'$$

$$(Ti^{IV}O^{2-}Ti^{IV})\text{–}OH_2 + h^+_{BV} \longrightarrow (Ti^{IV}O^{2-}Ti^{IV})\text{–}OH^{\bullet} + H^+$$

$$O_{2(ads)} + e^-_{BC} \longrightarrow O^{-\bullet}_{2(ads)}$$

1972, Fujishima i Honda otkrivaju da je moguća fotoelektroliza vode na elektrodi od $TiO_2$
Fujishima A. and Honda K, *Nature* 1972 (37) 238);

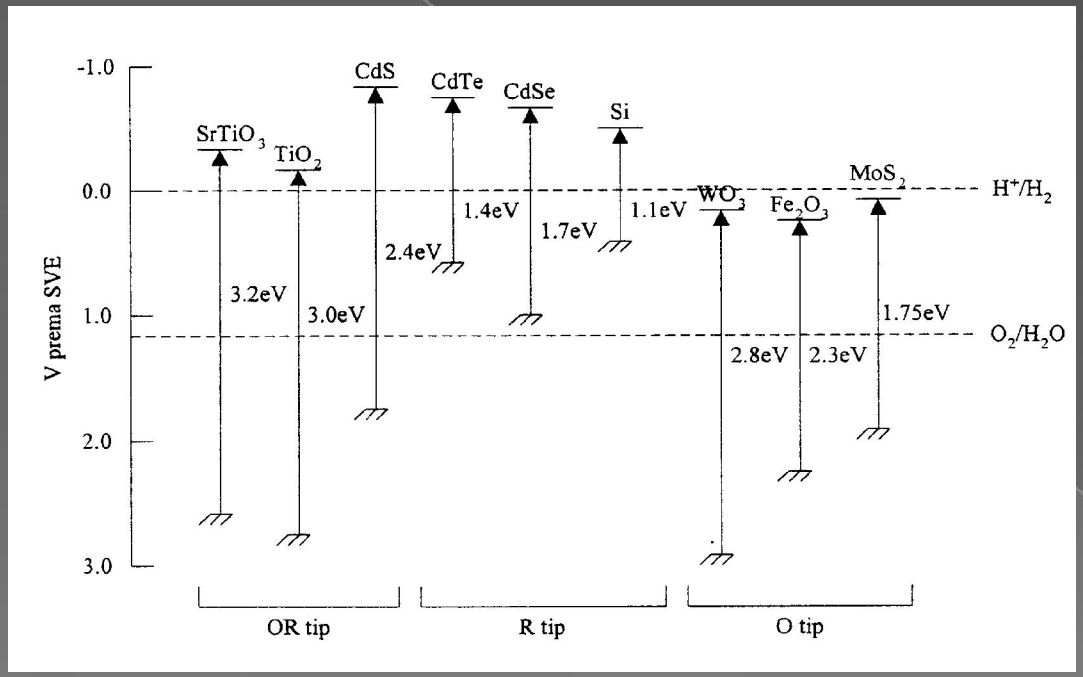


$\Delta G$= -237 kJ $mol^{-1}$ (2 x 1.23 eV)

OX: $2h^+ + H_2O \rightarrow 2H^+ + 1/2\ O_2$

RED: $2e^- + 2H^+ \rightarrow H_2$

U: $H_2O \rightarrow H_2 + 1/2O_2$

-upotreba $TiO_2$ za razgadnju organskih jedinjenja, (Fox,M.A *Acc Chem Res* **1983** (16) odnosno za prečišćavanje otpadnih voda i zagadjenog vazduha, (Schiavello,M, Ed. *Photocatalysis and Envi*. **1988** i M. Kaneko and I. Okura, Eds. Photocatalysis Science and Technology).

-heterogena fotokataliza počinje da se primenjuje i u organskoj sintezi, (Fox,M.A *J. Org. Chem.* **1989**, (54) 3847)

-D. Bahnemann posvećen primeni fkp za razgradnju polutanata (Solar Energy 77 **(2004)** 445–459).

Advantages on nanoscale:
large surface area – significant quantity of electrons can be exchanged between phases

Gratzel cell:

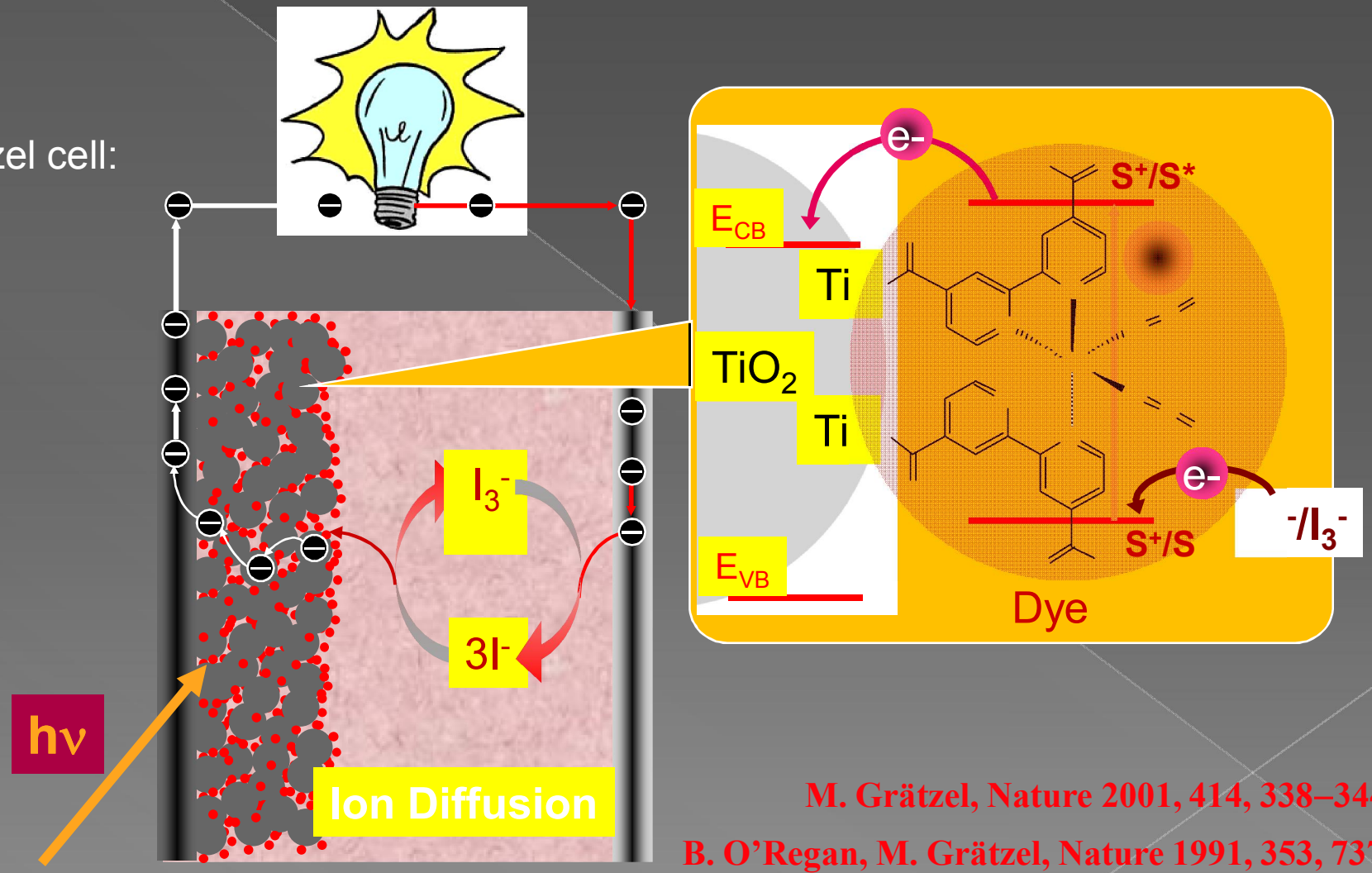


M. Grätzel, Nature 2001, 414, 338–344.

B. O'Regan, M. Grätzel, Nature 1991, 353, 737–740

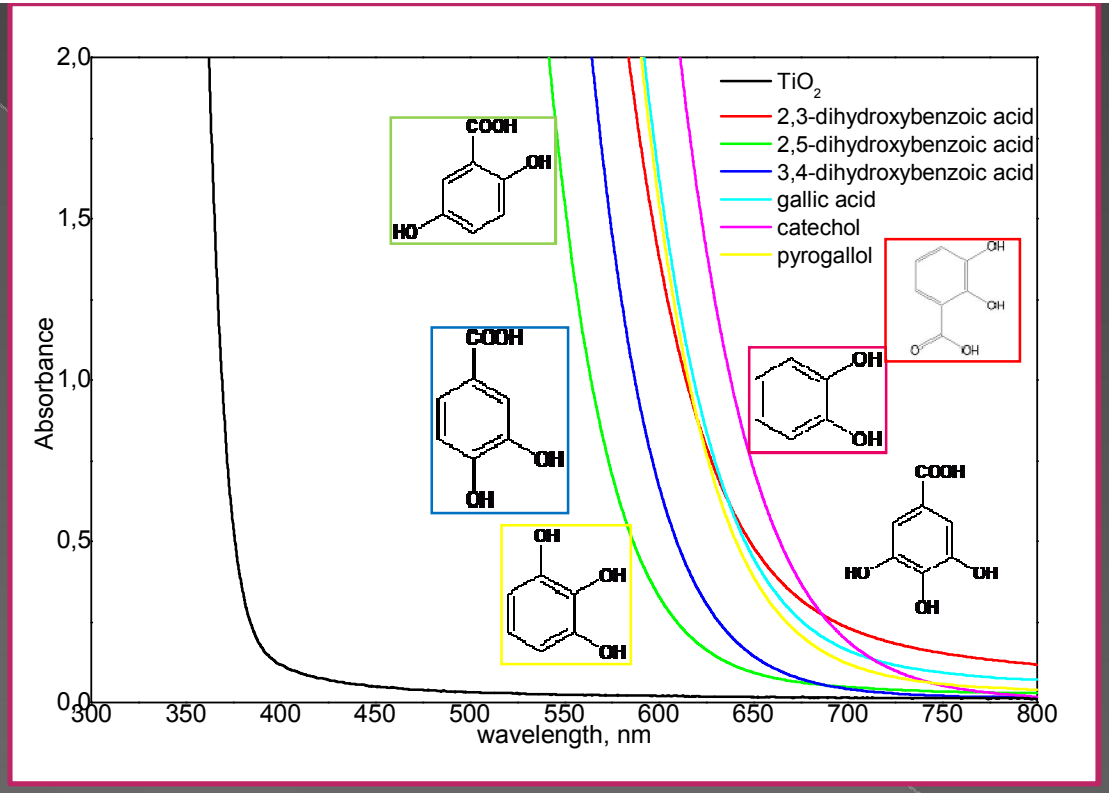


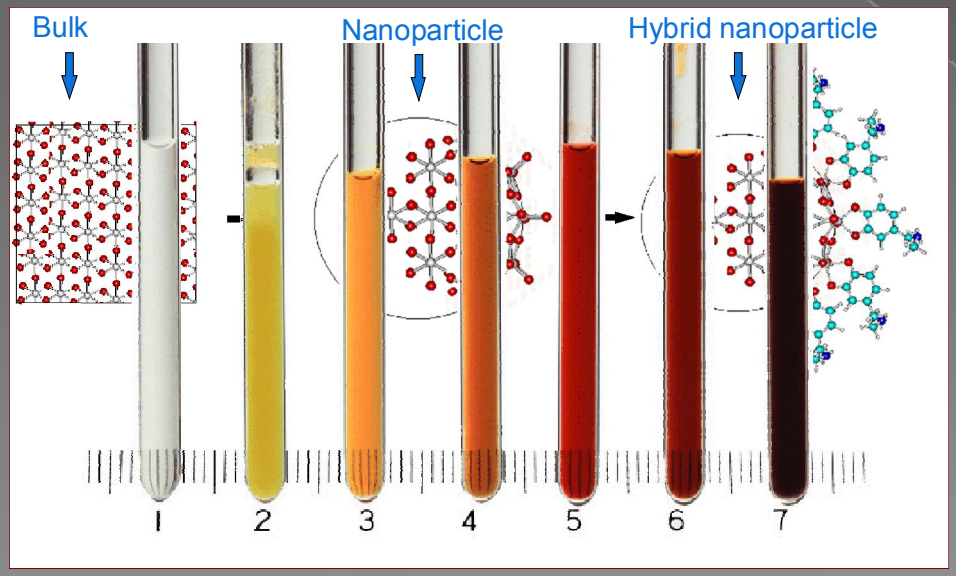

# Toward Electronic Coupling of Nanoparticles

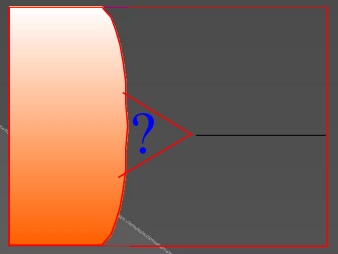


What is the link that allows efficient $e^-/h^+$ transfer?

Coupling of electronic properties of nanoparticles with molecules requires molecular understanding of surface sites:

## *Surface Sites Of Nanocrystalline Metal Oxides*

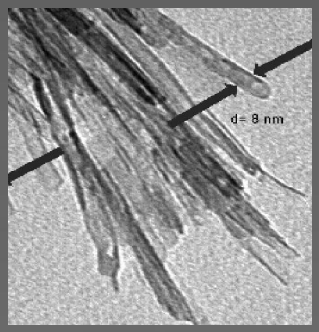


Octahedral
500 Å

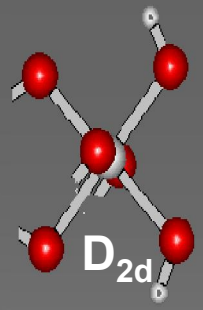


Square-pyramidal
19 Å

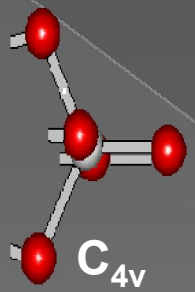


Octahedral
19 Å surface modified

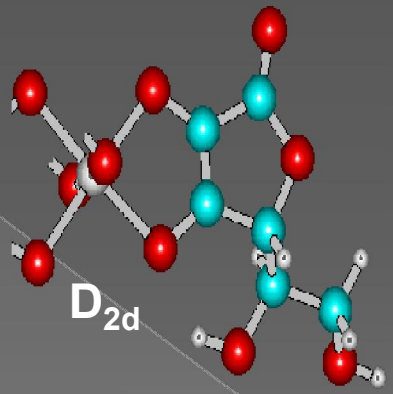


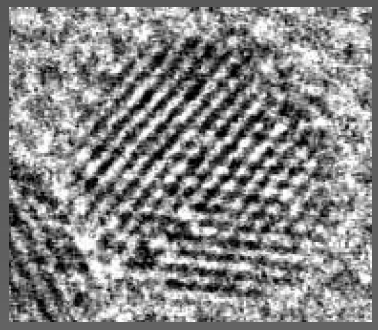

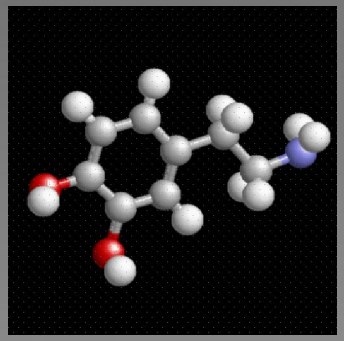

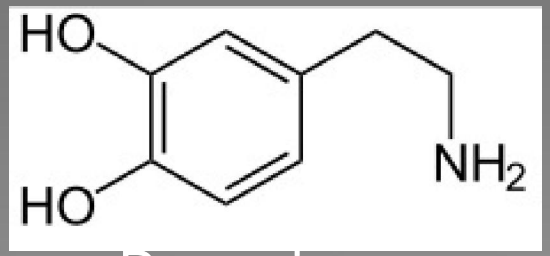


Dopamine

In nanosize regime reconstruction of the surface results in undercoordinated sites.

Unique and selective reactivity of nanoparticles

Adsorption induced healing of surface sites and tunable shift of abosrption

# Universal for high curvature surfaces of octahedral metal oxide nanoparticles, also $Fe_2O_3$, $ZrO_2$

## Healing of surface defect sites as dopamine binds

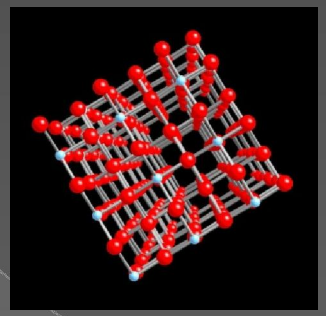

1/d = 2.64 $nm^{-1}$

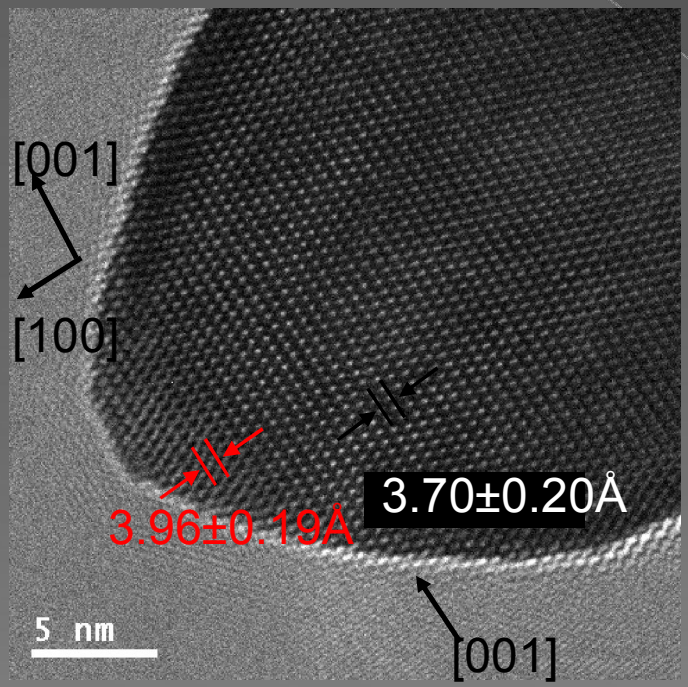


DA

Enediol ligand

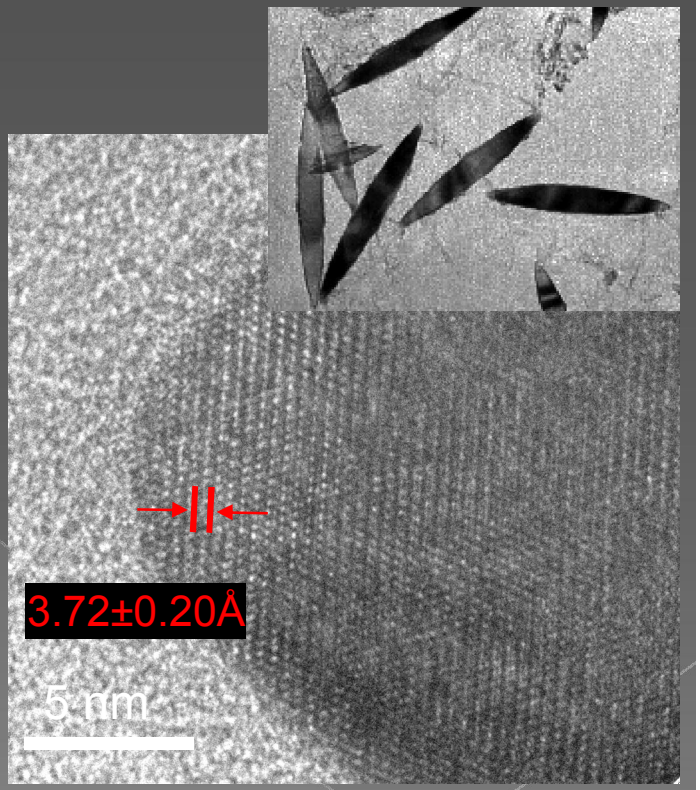


d

-five outermost atomic layers along [100] direction lattice spacing became longer;
-spacing of [104] and [102] planes became shorter;
-spacing in the [110] direction is unaffected;

The monochromatically tunable X-ray source for measuring an X-ray absorption spectrum (XAS) is synchrotron radiation, which covers all the wavelengths of the electromagnetic spectrum with an intensity of more than 100 times higher than the conventional X-ray tubes, used for crystallography or X-ray diffraction instruments.

The source is optimized to put large quantities of high-energy photons into a very small area in a very short time.

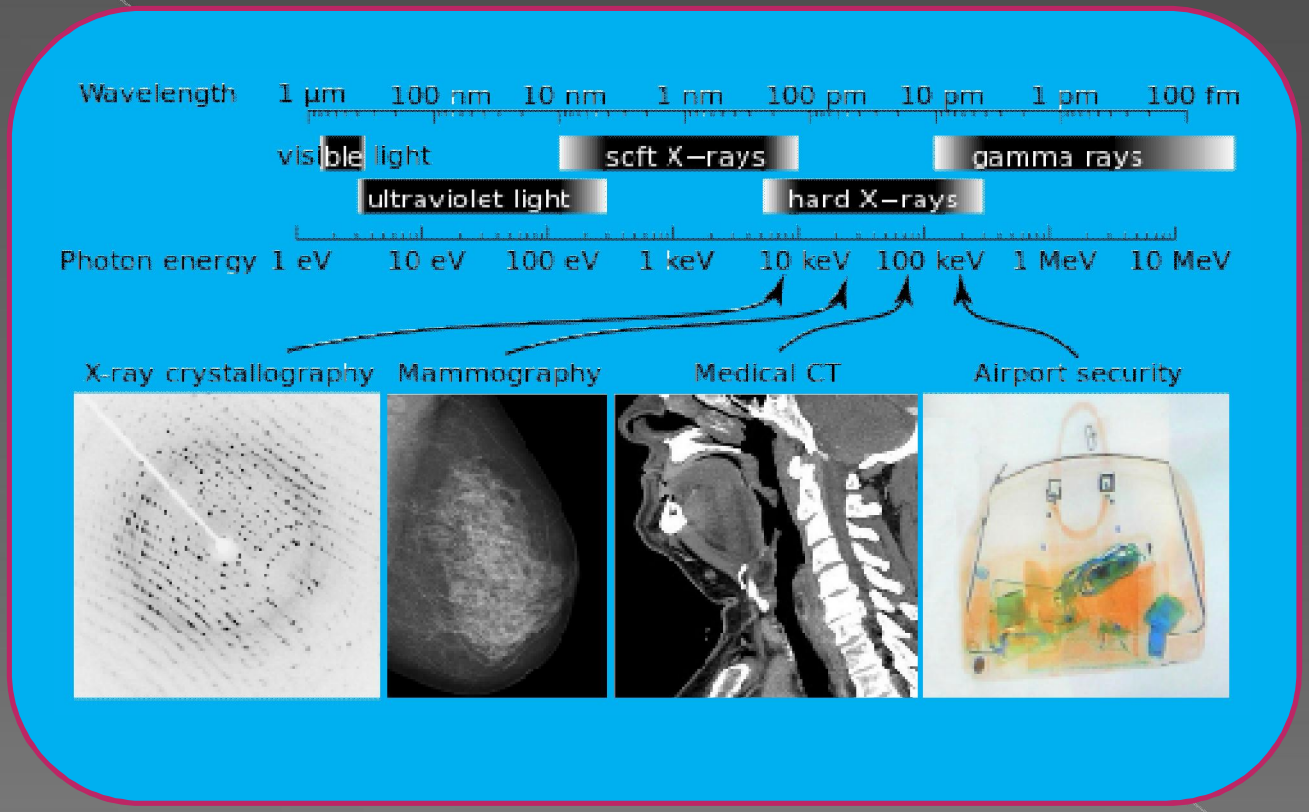


The energies used range from relatively "soft" x-rays (3-5 keV) to "hard" x-rays at 100 keV and sometimes higher.

## A. Linear Accelerator

Producing **brilliant x-ray beams** begins with electrons emitted from a **cathode heated to ~1100° C**. The **electrons are accelerated** by high-voltage alternating electric fields in a linear accelerator (linac) **to 450 million volts (MeV).**

At 450 MeV**, the electrons are relativistic: they are traveling at >99.999% of the speed of light (299,792,458 meters/second)**

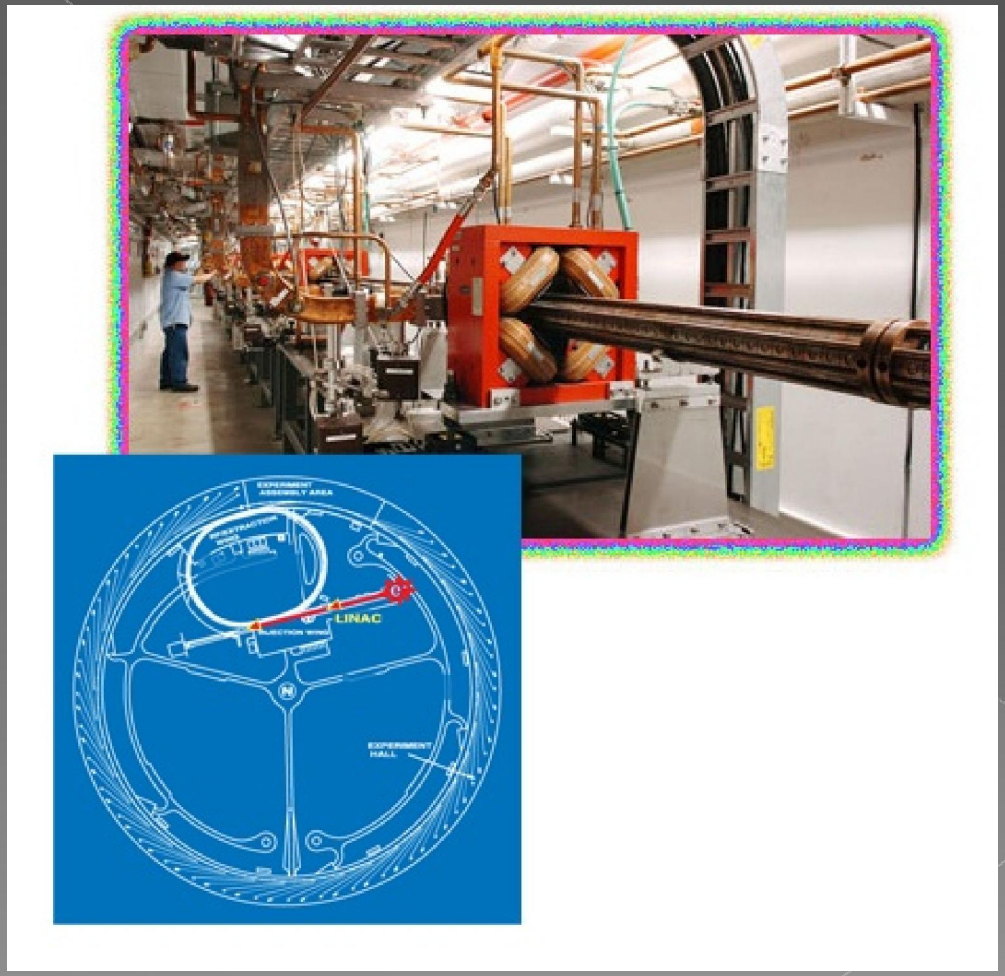

## B. The Booster Synchrotron

**Electrons are injected into the booster synchrotron** (photo below), a racetrack-shaped ring of electromagnets, and **accelerated from 450 MeV to 7 billion electron volts (7 GeV) in one-half second**. (By comparison, the electron beam that lights a TV screen is only 25,000 electron volts.) **The electrons are now traveling at >99.999999% of the speed of light.** The accelerating force is supplied by electrical fields in four radio frequency (rf) cavities. **In order to maintain the orbital path of the electrons, bending and focusing magnets increase the electron field strength in synchronization with the rf field.**

## C. The Electron Storage Ring

The 7-GeV electrons are injected into the 1104-m-circumference storage ring, a circle of more than 1,000 electromagnets and associated equipment,

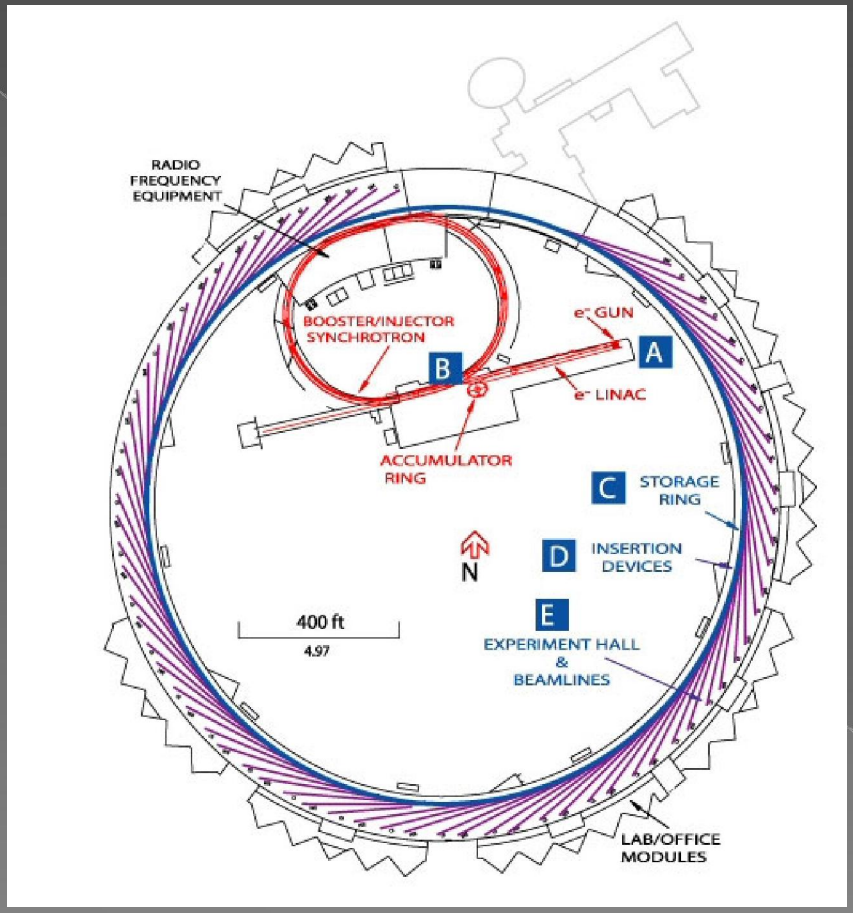


A powerful electromagnetic field focuses the electrons into a narrow beam that is bent on a circular path as it orbits within aluminum-alloy vacuum chambers running through the centers of the electromagnets.

# X-Ray Absorption Spectroscopy

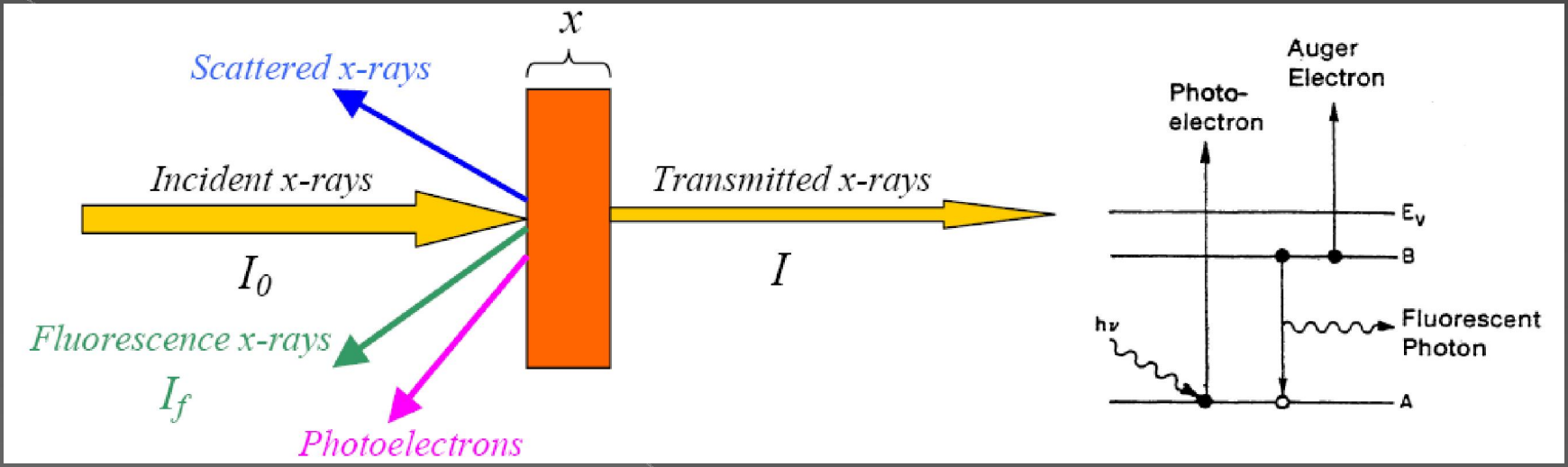


A narrow parallel monochromatic x-ray beam of intensity **$I_0$ passing through a sample of thickness x will get a reduced intensity I according to the expression:**

$$\ln (I_0 / I) = \mu x$$

where μ is the linear absorption coefficient, which depends on the types of atoms and the density ρ of the material.

The XAS principle is based on the determination of the x-ray absorption coefficient (μ) depending on the photon energy (hv) at a fixed angle of illumination θ.

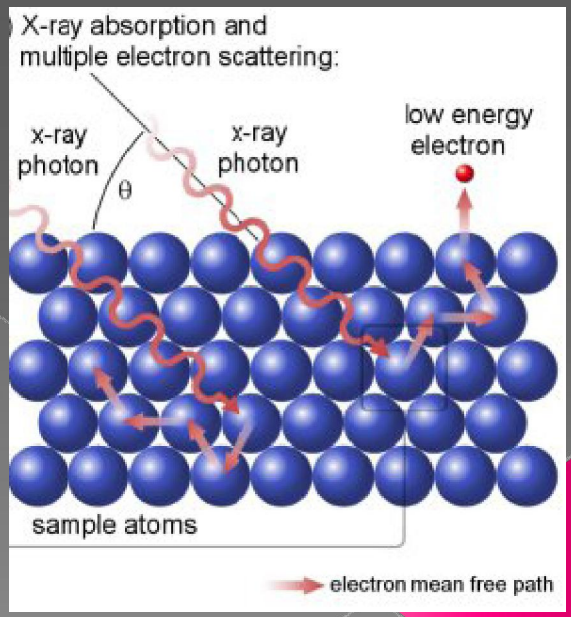

At certain energies where the absorption increases drastically, and gives rise to an absorption edge.

Each such edge occurs when the energy of the incident photons is just sufficient to cause excitation of a core electron of the absorbing atom to a continuum state, i.e. to produce a photoelectron.

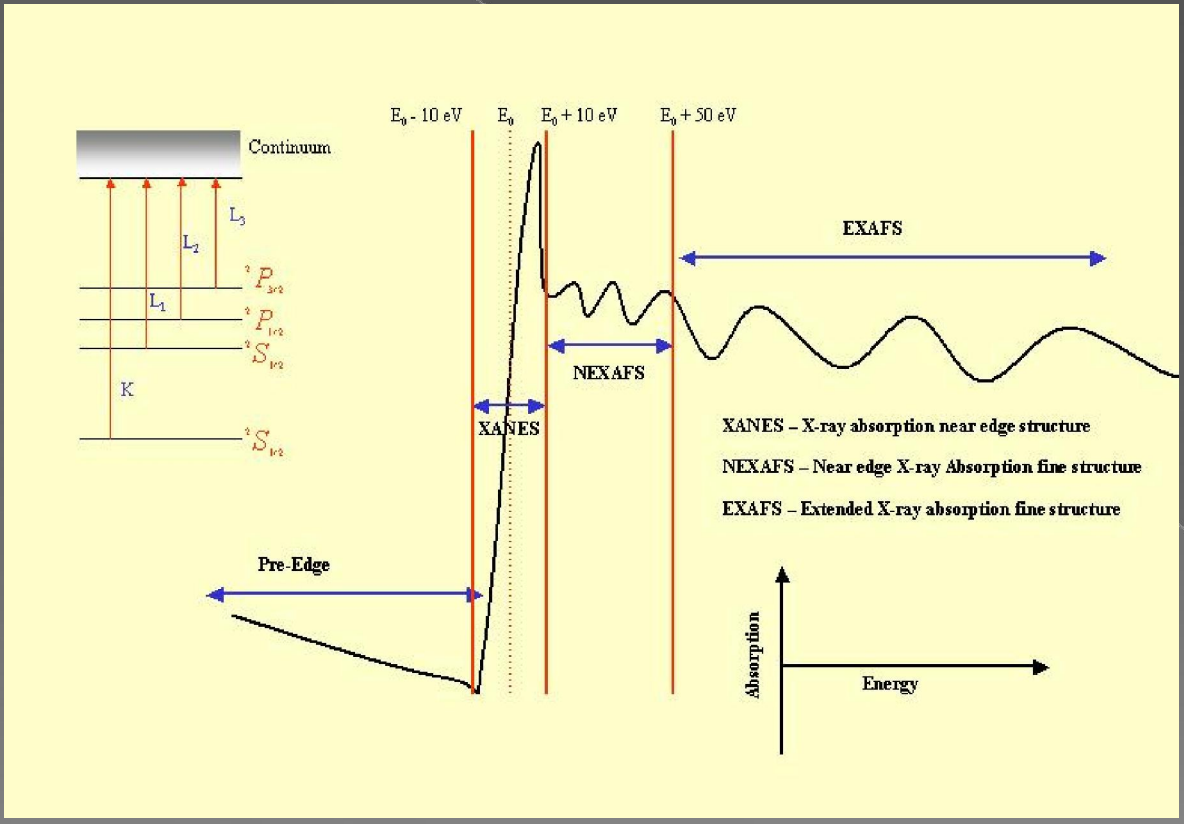


Thus, the energies of the absorbed radiation at these edges correspond to the binding energies of electrons in the K, L, M, etc, shells of the absorbing elements.

The absorption edges are labelled in the order of increasing energy, K, $L^{I}$, $L^{II}$, $L^{III}$, $M^{I}$,…., corresponding to the excitation of an electron from the 1s ($^2S_{½}$), 2s ($^2S_{½}$), 2p ($^2P_{½}$), 2p ($^2P_{3/2}$), 3s ($^2S_{½}$), … orbital (states), respectively.

Beyond the absorption edge the intensity of a monochromatic x-ray passing through a medium of thickness d will follow the absorption law

$$I \propto \exp(-\mu d) \quad , \quad \mu \propto \frac{Z^x}{(h\nu)^3} \quad , \quad 3 < x < 4,$$

Whereby μ depends the atomic number Z of the medium and decreases with increasing photon energy hv

An x-ray absorption spectrum (XAS) can be measured in two different ways:

1) **Transmission mode**, where the intensity of the x-ray beam is measured before ($I_0$) **and after passing through the sample** ($I_1$) using ion chamber gas detectors. **Here, the number of x-ray photons absorbed by core electrons to create a photoelectron (and a "hole") is counted.**

   **The XAS spectrum will then show the variation of** $(\log I_0 / I_1)$ **vs. energy (eV).**

2) **Fluorescence mode** is used e.g. when:

   i) the sample is dilute and the variation of $(\log I_0 / I_1)$ **is small;**

   **ii) there is high "self-absorption" by sample matrix.**

   **The fluorescence radiation** ($I_f$) **from the sample is then measured, using a Lytle or Germanium detector, as a secondary effect of the x-ray absorption. Here, the number of fluorescent photons emitted from the sample, when an electron in the upper level fills the "hole" in the core level, is counted.**

   **The XAS spectrum shows the variation of** $(I_f / I_0)$ **vs. energy (eV)**

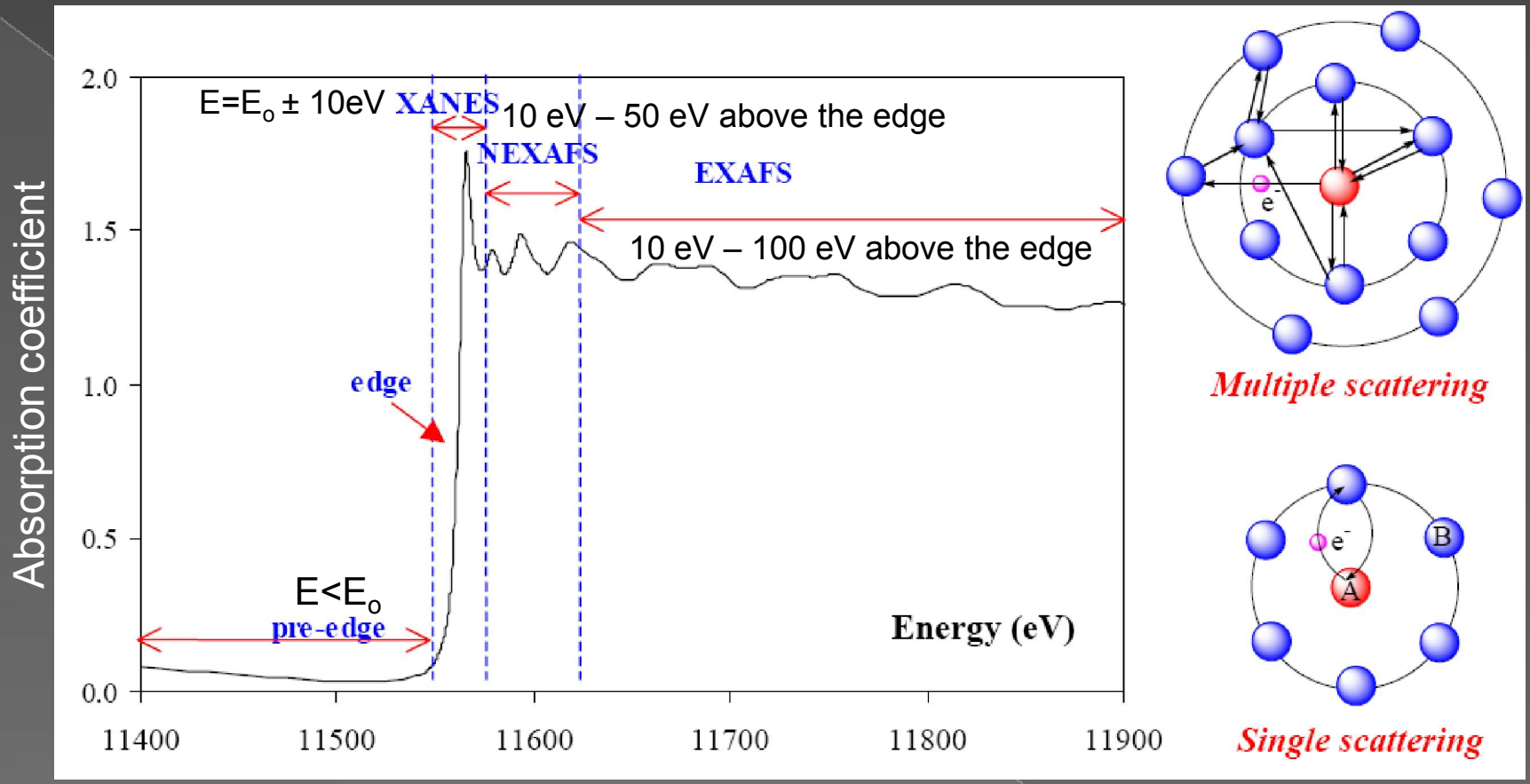


-Minor features in the pre-edge region are usually due to the electron transitions from the core level to the higher unfilled or half-filled orbital (e.g., *s* → *p*, or *p* → *d*).

-In the XANES region, transitions of core electrons to non-bound levels with close energy occur.

-In NEXAFS, the ejected photoelectrons have low kinetic energy (E-E$_o$ is small) and experience strong multiple scattering by the first and even higher coordinating shells.

-In the EXAFS region, the photoelectrons have high kinetic energy (E-E$_0$ is large), and single scattering by the nearest neighboring atoms normally dominates. Detailed information about the local atomic structure.

The photoelectron will interact with the surrounding atoms.

**A schematic diagram of the radial portion of the photoelectron wave with a low kinetic energy (solid lines) being backscattered by the surrounding atoms (dotted lines)**

-backscattered waves interfere with the forward wave to produce either peaks or troughs.

The net result is a series of oscillations on the high photon energy side of the absorption edge.

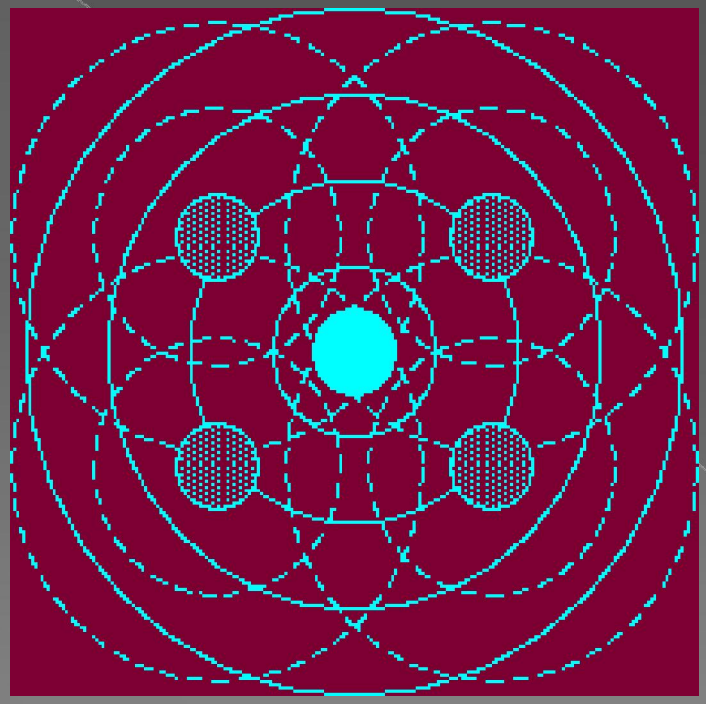

**-since backscattering amplitude and phase are dependent on the type of atom doing the backscattering and the distance it is from the central atom, information regarding the coordination environment of the absorbing atom can be obtained by analyzing the EXAFS.**

This powerful technique for probing the local structure around almost any specific element in the periodic table (except the lightest) gives information on the number and chemical identities of near neighbors and the average inter-atomic distances up to 5-6 Å.

**EXAFS** studies can be performed at trace levels (<1000 ppm), which is useful e.g., for studying metal complexes on surfaces, catalysts and metal sites in bioinorganic samples.

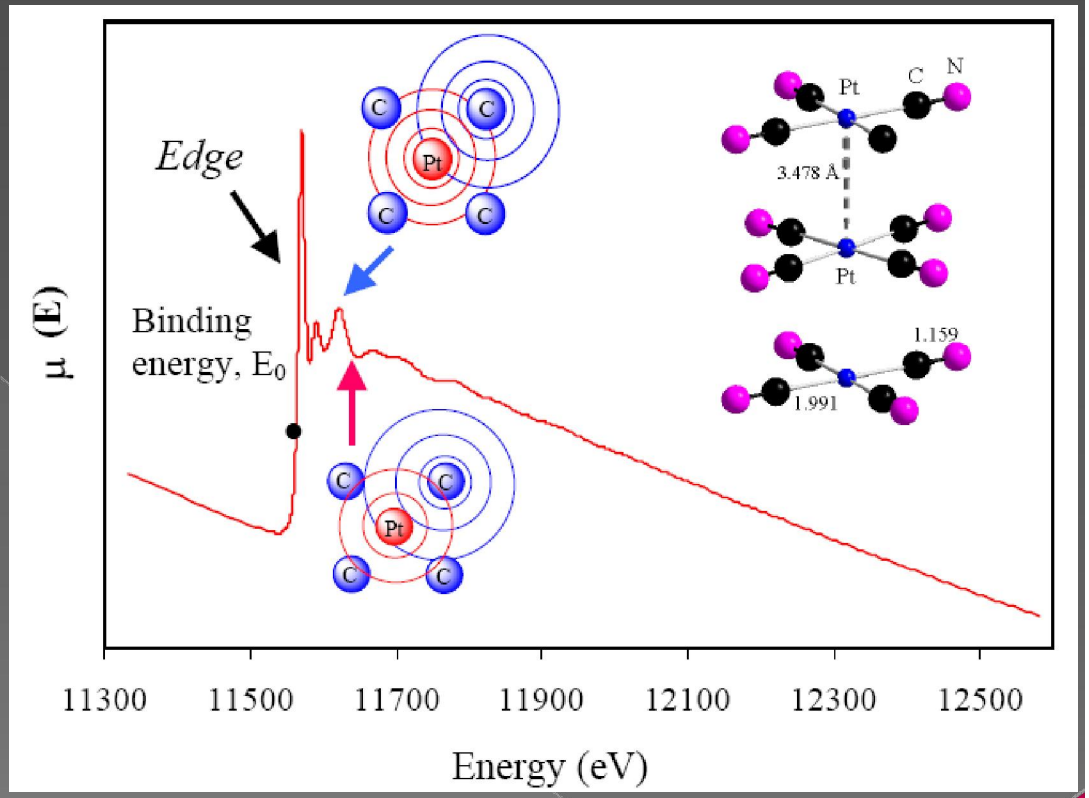

# X-ray Absorption Near Edge Structure (XANES) Spectroscopy

The near edge structure of an x-ray absorption spectrum is sensitive to the coordination, oxidation state and density of states of the absorbing atom.

For example, the XANES region of:
1 mM $Cr^{3+}$(aq) and 1 mM $[Cr^{6+}O^{4}]^{2-}$ (aq) are very different (M. Lytel, et al., Plant, **1998, 206, 293-299).**

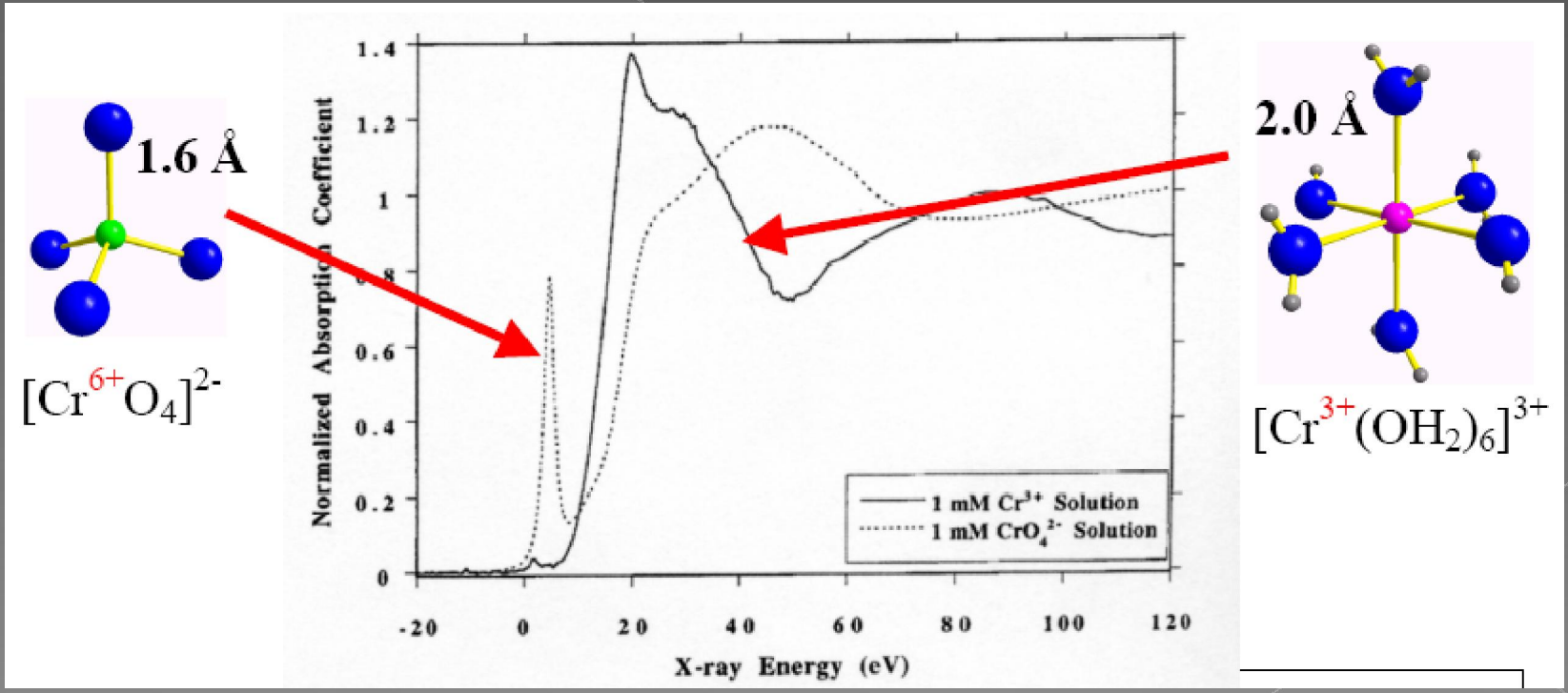

Sulfur has a rich XANES structure, with a 13 eV shift from S(-2) in sulfide to S(+6) in sulfate.

Comparison between the XANES spectra of equimolar solutions of elemental sulfur in p-Xylene, and $Na_2SO_4$ in water.

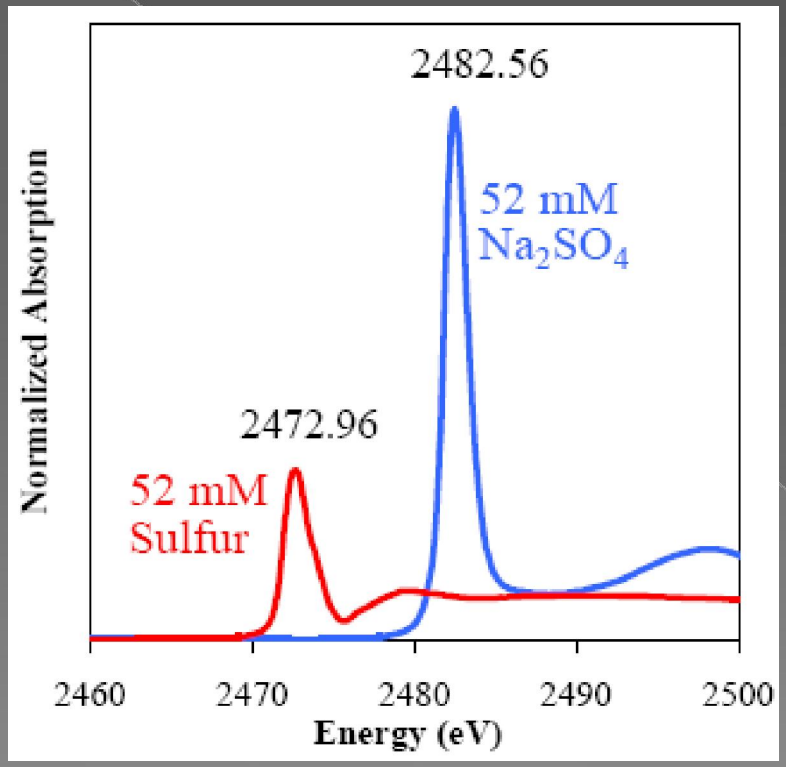


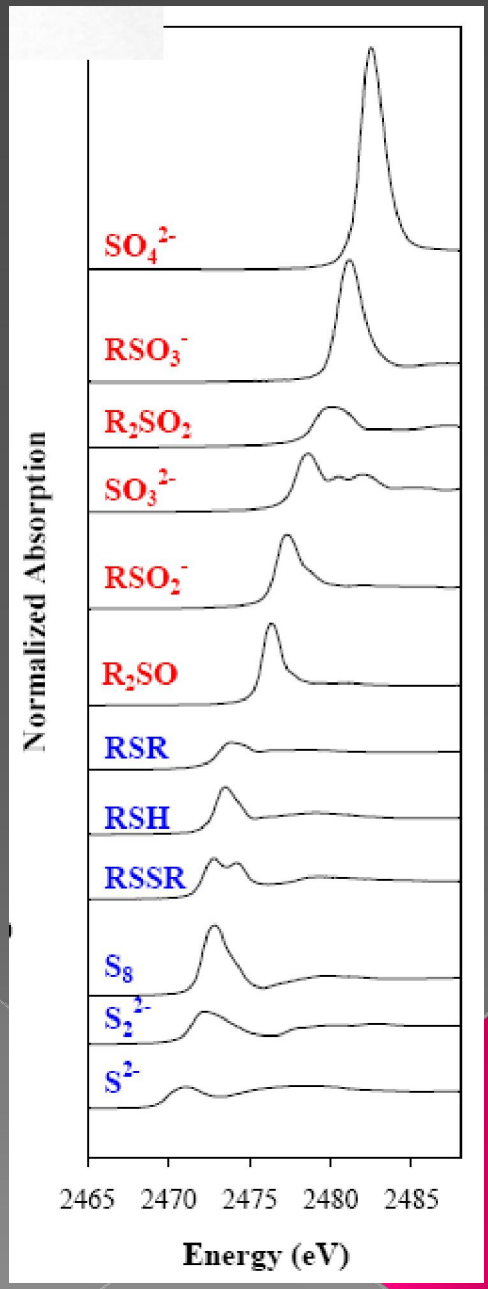

The main advantage of EXAFS analysis over X-ray Crystallography is that structures can be studied in non-crystalline forms (including liquid, gasses and frozen solutions).

- non-crystalline materials,

- metallo-proteins in their naturally occurring states.

- glasses

-distances between central and neighboring atoms,

-numbers of neighboring atoms, types and disorder

Complementary Structure Probes:

X-ray and Neutron diffraction
powerful and fast (x-ray), need good crystals, no solutions

2-D and higher dimensional NMR
Atomic resolution structures in solution, no large molecules, slow

XAFS
Gives short range structure around metal atom, slow.

XANES
probes orbital matrix elements and occupancy.

Related techniques:

XMCD: X-ray Magnetic Circular Dichroism
Uses circularly polarized x-rays to probe magnetic structure.

IXS: Inelastic X-ray Scattering
Analyzes the fluorescence radiation at high resolution, providing a 2-D excitation map. Provides a great deal of information in the near-edge region.

X-ray Raman
Essentially allows one to obtain XAFS like information using high energy x-rays

DAFS
Hybrid diffraction/XAFS gives sensitivity to nonequivalent sites in crystals and multilayers

XPS, ARPEFS, fluorescence holography...

*Reshaping of $TiO_2$ Nanotubes in neutral media (pH~7) and acidic media (pH<5) during additional hydrothermal process.*

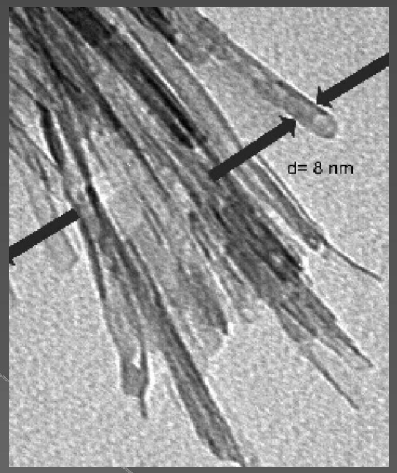


*Changing initial concentration of Nanotubes in neutral media results in Nanorods with different aspect ratios.*

*Length 200-300 nm*
*Radius 60-70 nm*

*Length 50-60 nm*
*Radius 20 nm*

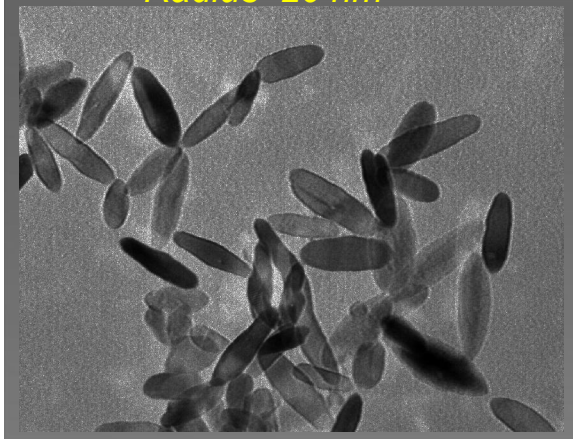

2h/250°C

*Rate of nucleation is higher than the rate of crystal growth*

*Rate of crystal growth is higher than the rate of nucleation*

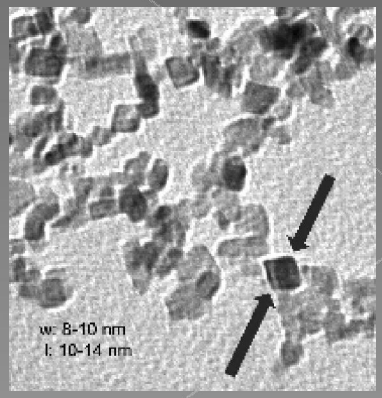


1-2h
150°C-250°C

*Reshaping of $TiO_2$ Nanotubes in acidic media (pH<5) results in faceted Nanoparticles*

# SMALL AND WIDE ANGLE X-RAY SCATTERING ( SAXS/WAXS )

-complementary methods for determining:

1) **size**,

2) **size distribution**

3) **structure**

of a wide range of disordered (non-crystalline or semi-crystalline) materials:

**polymers, liquid crystals, oils, suspensions and biological samples like fibers or protein molecules in solution.**

Small-angle X-ray scattering **(SAXS) low scattering 2θ angles (1-10°)** in **the size range 2-200** nm

- This angular range contains information about the shape and size of macromolecules, characteristic distances of partially ordered materials, pore sizes, and other data.
- SAXS is capable of delivering structural information of macromolecules between 5 and 25 nm, of repeat distances in partially ordered systems of up to 150 nm. USAXS (ultra-small angle X-ray scattering) can resolve even larger dimensions.

Wide-angle X-ray scattering **(WAXS) routinely covers the angular range 5-60° resolution with precision of 0.1A in the size range 1-100 nm.**

Data presented in **momentum transfer, q (q=4¶sinθ/λ),** Θ is the one-half of the scatered angle.

**λ = 0.67** Å at **20 keV** energy probing X-ray in the range of 0-6 $Å^{-1}$

There is no inhomogeneity raised by the presence of $Mn^{2+}$ ions or indication of MnO clustering

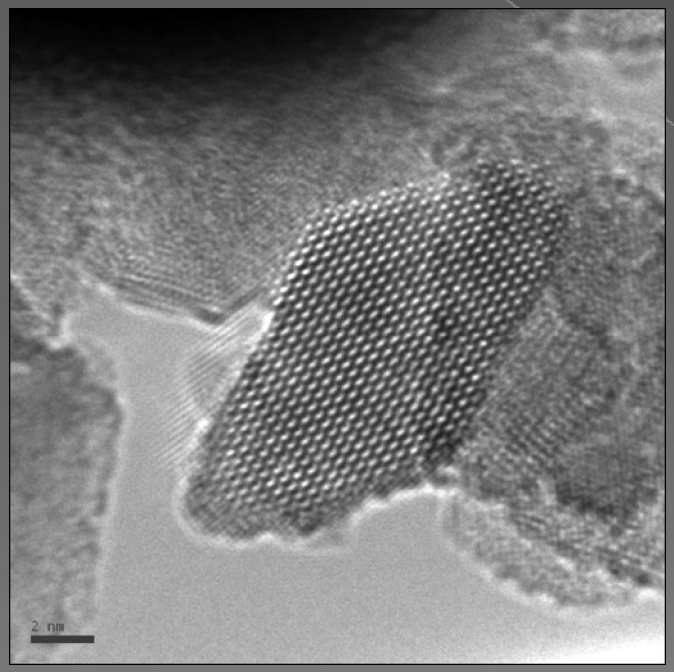


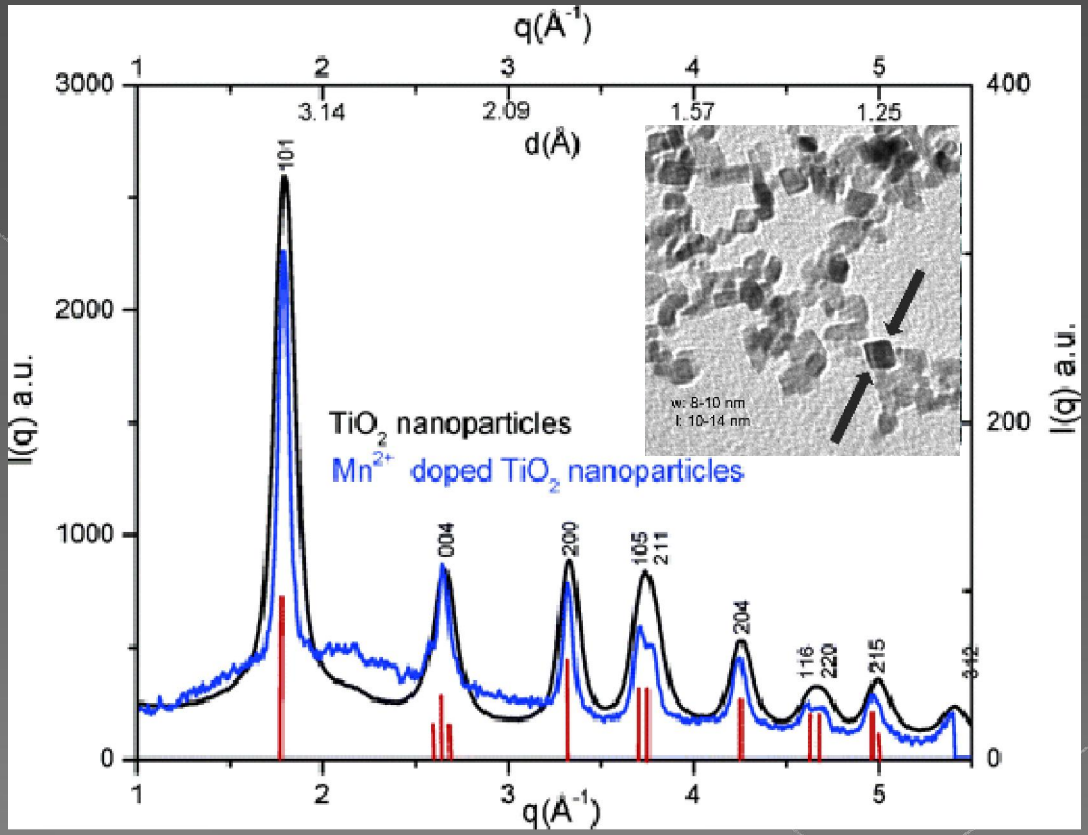


There is still possibility of local distortions due to slightly larger $Mn^{2+}$ ions and significantly different charge from that of the Ti atoms.

Substitutional or interstitial sites?

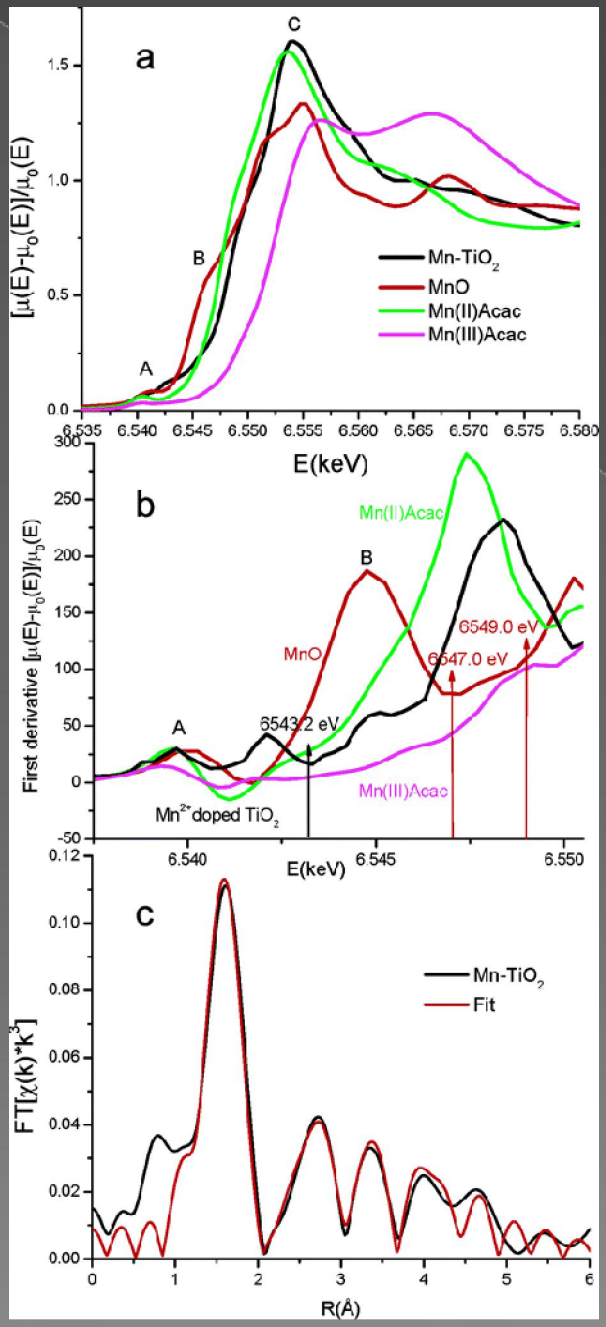


## Mn K-edge XANES spectra

The valence of the $Mn^{2+}$ ion is retained after incorporation Mn;

K-edge jump at 6.549 keV.

**6.547 keV in MnO** is consequence of constructive and destructive interferences related to Mn distant neighbors 5-6.5 Å around central Mn atoms.

Appearance of the peak at **6.5432 keV** confirm successful Incorporation of mainly isolated $Mn^{2+}$ Ions into $TiO_2$. New electronic properties due to contributions of Ti distant neighbors.

Average Mn-O bond length is 0.1-0.14 Å longer than the Ti-O bond length in undoped anatase $TiO_2$

**Coordination numbers are not changed drastically**

**There is no evidence of Mn clustering**

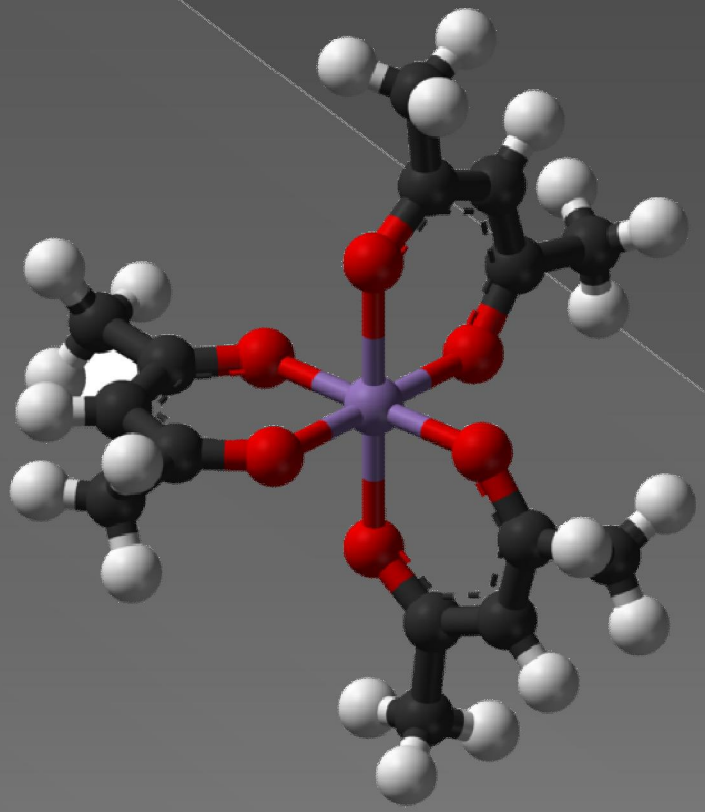

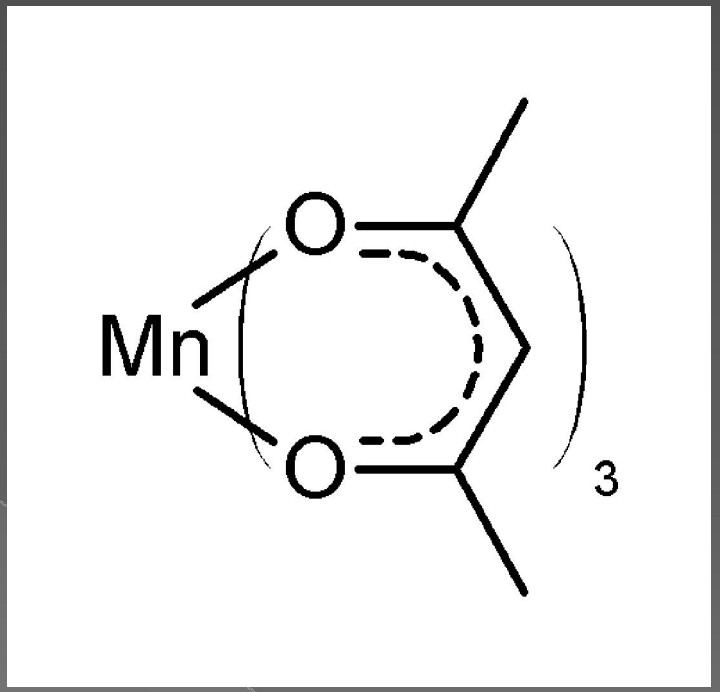

**Continuous wave electron paramagnetic resonances (EPR) spectroscopy:**

- **presence** of magnetically isolated $Mn^{2+}$ dopants in $TiO_2$ matrix;

- interaction **of photogenerated charge carriers from $TiO_2$ with substitutional Mn atoms;**

-EPR spectroscopic technique

detects species that have unpaired electron:

free radicals,
transition metal ions
defects in materials

-free electrons are often short-lived, but still play crucial roles in many processes:

- photosynthesis
- oxidation
- catalysis
- polymerization reactions.

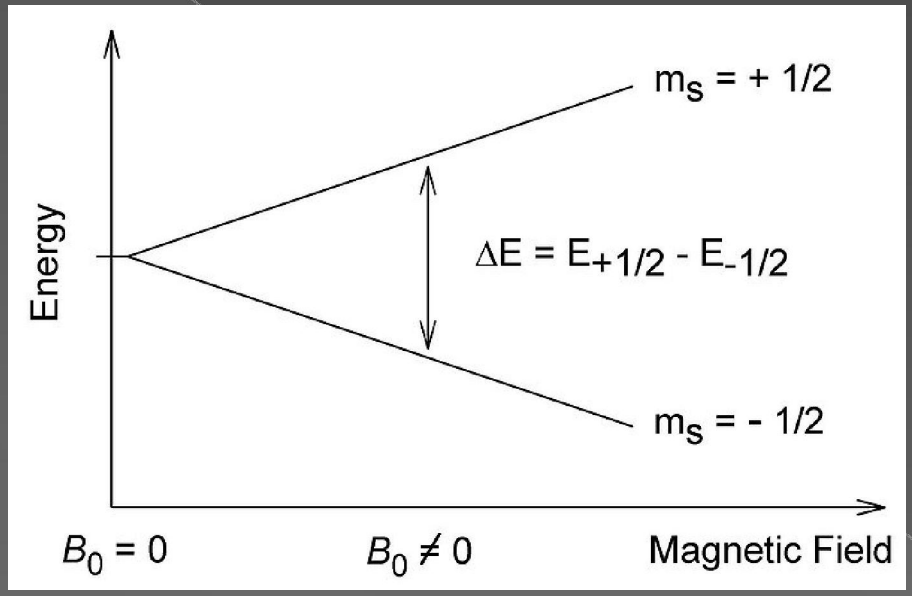


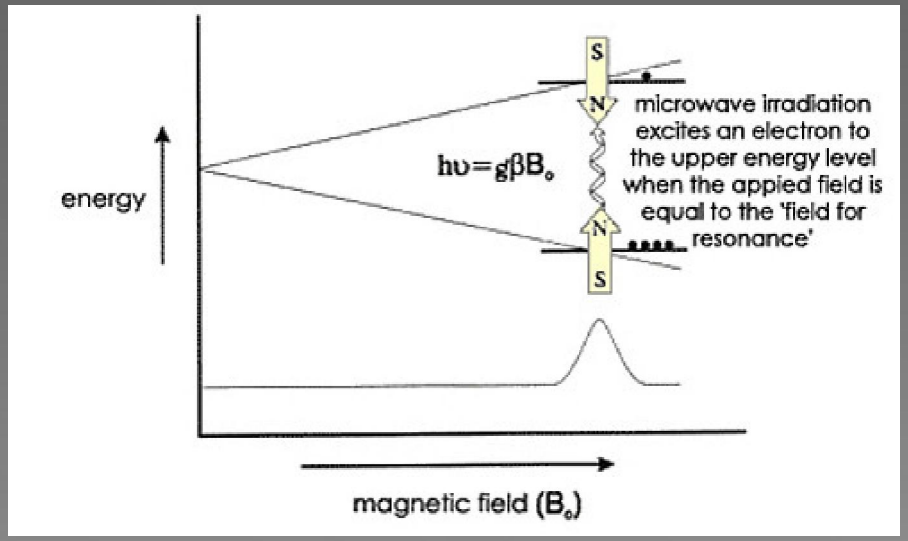


**How does EPR work?**

-EPR is a **magnetic resonance technique** similar to NMR.

-like a proton, the **electron has spin**, which gives it a magnetic property known as a **magnetic moment** ($m_s$=+1/2; $m_s$=-1/2).

-when we supply an external magnetic field, the **paramagnetic electrons can either orient in a direction parallel** ($m_s$=-1/2) **or antiparallel** ($m_s$=+1/2) **to the direction of the magnetic field**.

This creates **two distinct energy levels** for the unpaired electrons and allows us to measure them as they are driven between the two levels.

-we are **detecting the transitions of unpaired electrons in an applied magnetic field**.

Microwaves frequencies in the range of: 9000 – 10000 MHz (9 – 10 GHz)
Magnetic fields corresponding to about 3500 G (0.35 T).

A collection of paramagnetic centers, such as free radicals, is exposed to microwaves at a fixed frequency.

By increasing an external magnetic field, the gap between the $m_s$ = +1/2 and $m_s$ = −1/2 energy states is widened until it matches the energy of the microwaves. At this point the unpaired electrons can move between their two spin states.

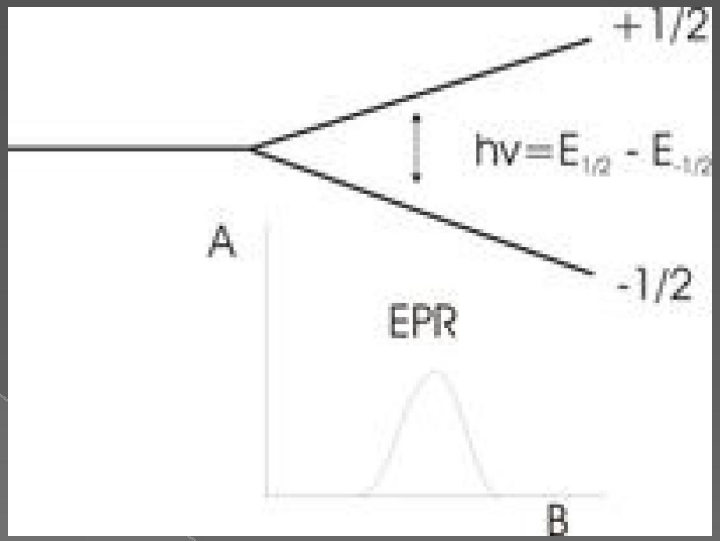


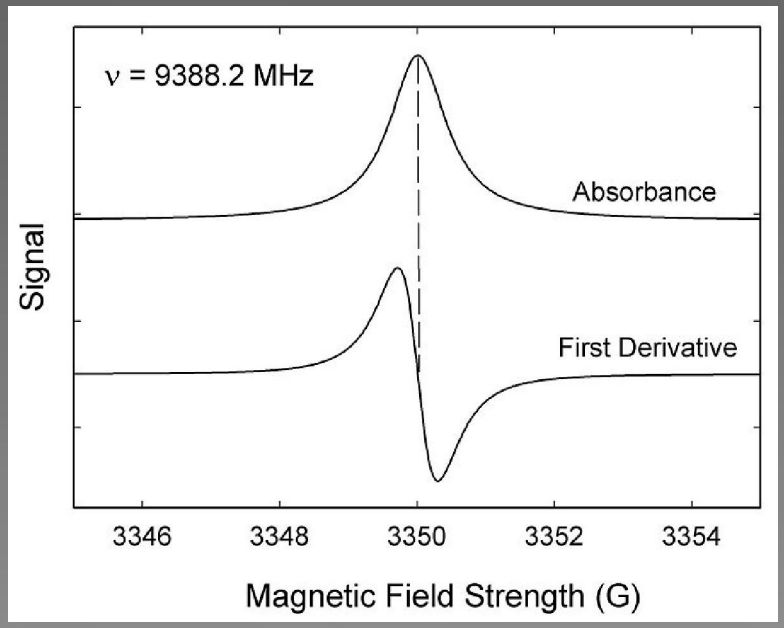


Since there are typically more electrons in the lower state, due to the Maxwell-Boltzmann distribution here is a net absorption of energy, and it is this absorption which is monitored and converted into a spectrum.

Fundamental equation of EPR spectroscopy: $h\nu = g_e \mu_B B_0$

where $g_e$ is the gyromagnetic ratio of the electron (Landé *g*-factor) the ratio of its magnetic dipole moment to its angular momentum, and $\mu_B$ is the Bohr magneton.

An unpaired electron responds not only to a spectrometer's applied magnetic field $B_o$, but also to any local magnetic fields of atoms or molecules. The effective field $B_{eff}$ experienced by an electron is thus written:

$$B_{eff} = B_o(1-\sigma)$$

where $\sigma$ includes the effects of local fields ($\sigma$ can be positive or negative).

Therefore, the $h\nu = g_e \mu_B B_{eff}$ resonance condition (above) is rewritten as follows:

$$h\nu = g_e \mu_B B_{eff} = g_e \mu_B B_o(1-\sigma)$$

The quantity $g_e(1 - \sigma)$ is denoted *g* and called simply the *g*-factor:

$$h\nu = g \mu_B B_o$$

A free electron has a *g* value of 2.002319304386 (electronic *g*-factor).
For radiation at the commonly used frequency of ca. 10 GHz (microwave X-band), resonance occurs at a magnetic field of about 0.34 Tesla (3400 Gauss).

If an atom with which an unpaired electron is associated has a non-zero nuclear spin, then its magnetic moment will affect the electron. This leads to the phenomenon of hyperfine coupling, analogous to J-coupling in NMR, splitting the EPR resonance signal into doublets, triplets and so forth.

The *g*-factor and hyperfine coupling in an atom or molecule may not be the same for all orientations of an unpaired electron in an external magnetic field. This anisotropy depends upon the electronic structure of the atom or molecule (e.g., free radical) in question, and so can provide information about the atomic or molecular orbital containing the unpaired electron.

Only EPR detects unpaired electrons unambiguously.

**EPR** samples are very **sensitive to local environments**. Therefore, the technique sheds light on the molecular structure near the unpaired electron or incorporated dopants.

-due to the exchange interactions between paramagnetic ions and their neighbors, **paramagnetic ions report on their electronic couplings with adjacent lattice atoms**.

-sometimes, the EPR spectra exhibit dramatic line shape changes, giving insight into their chemical nature, oxidation state and the local symmetry.

-**coupled with light excitation**, EPR reveals the **energetics** and **reactivity** of selected atoms in the different environments.

# $Mn^{2+}$ ions ($3d^5$, electron spin S=5/2)

The number of lines in EPR spectrum=2MI+1
M-number of nuclei; I- nuclear spin

The EPR spectrum of $Mn^{2+}$ consists of six hyperfine lines due to weak magnetic interaction between its unpaired electrons and the manganese nucleus.

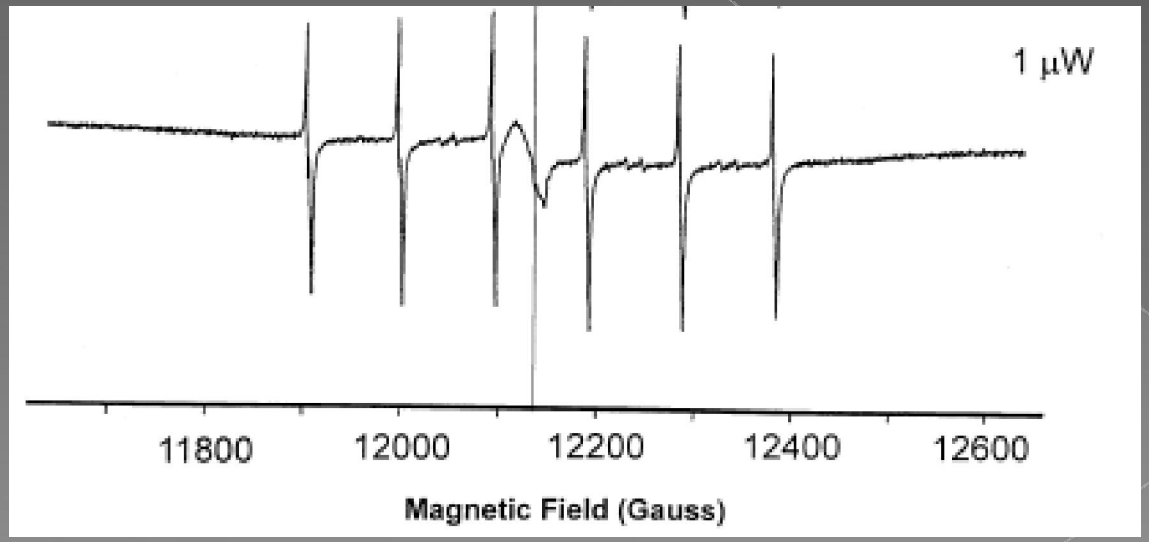

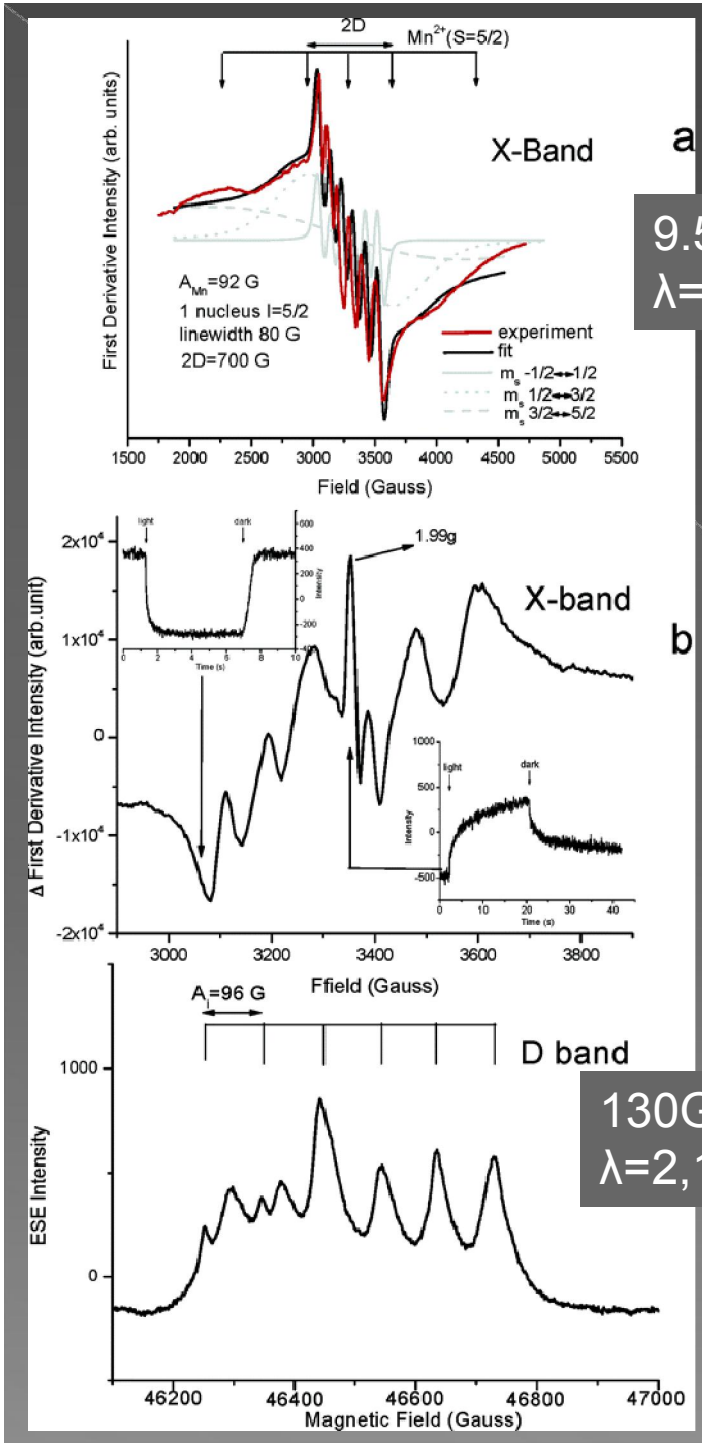


-Hyperfine splitting ($^{55}Mn$ nucleus, nuclear spin I=5/2) is superimposed on broad resonances of the fine structure of $Mn^{2+}$ broadened due to their strong angular dependence.

six resonance lines correspond to allowed ($\Delta m_I=0$) hyperfine ransitions between Zeeman sublevels ($m_s=\pm 1/2$)

-Hyperfine splitting constant $A_{iso}$

**-Presence of fine structure is indication of relative ordering between Mn dopants**

-upon illumination a decrease of all spectral features associated with manganese signal was observed

-$Mn^{2+}$ dopant atoms participate as electron-donating centers in the process of light excitation

$$TiO_2{:}Mn(II) \xrightarrow{h\nu} Mn(III) + xe_{cb}^{-} + (1-x)Ti(III)$$

-two sets of hyperfine sextets indicating two species in different coordination geometry

**-Octahedral coordination, $A_{iso}$=86G, of $Mn^{2+}$ ions in bulk.**

**-Undercoordinated geometry, $A_{iso}$=96G, of $Mn^{2+}$ ions within surface of nanocrystals.**

# High field EPR D-band derivative spectra recorded at different temperature

## D band λ = 2,1 mm; v = 130 GHz

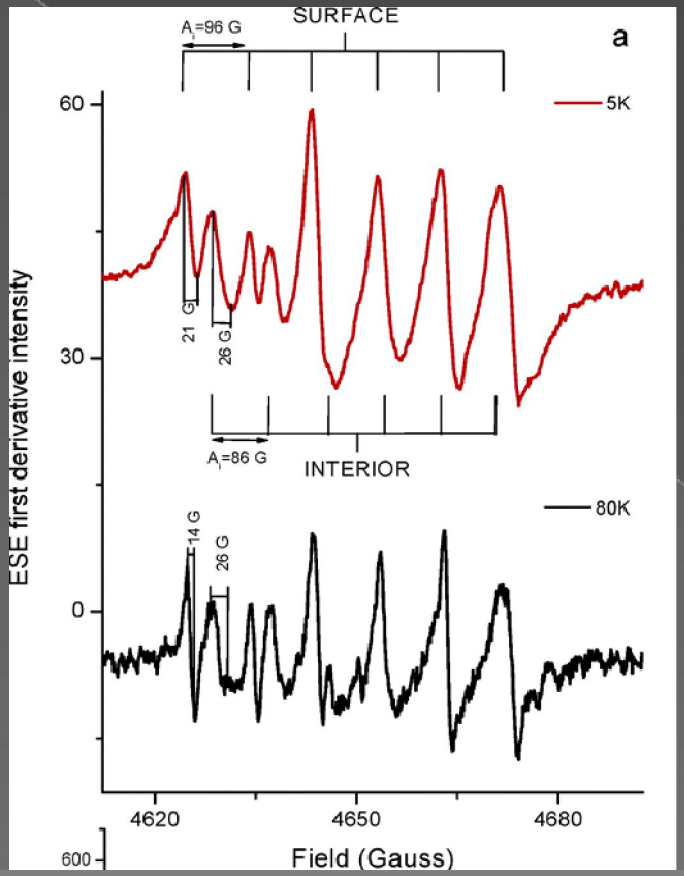


-line width of the spectrum having larger hyperfine constant (undercoordinated surface sites) decrease faster with temperature;

-species within surface relaxes much faster than the one in a bulk;

**-faster relaxation suggests stronger exchange interaction of Mn atoms with host matrix i.e.electronic states of anatase lattice.**

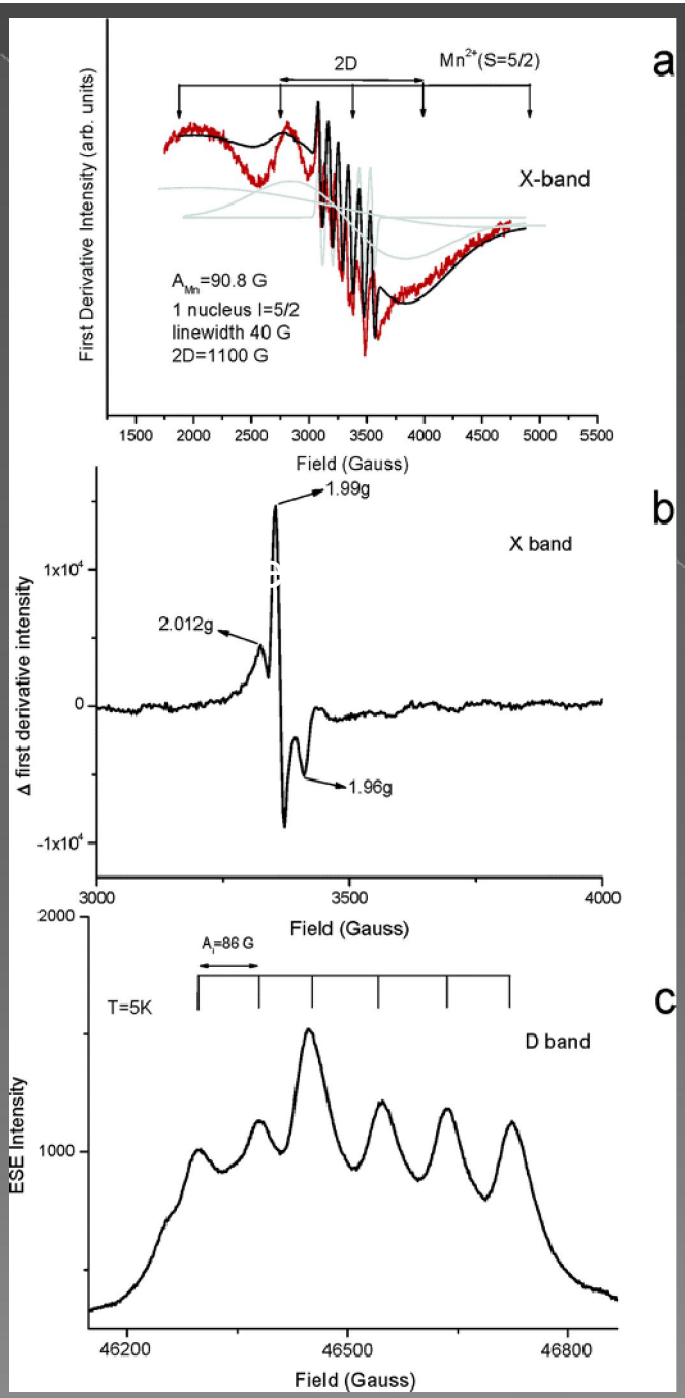


## Dialyzed sample

-one sextet of lines with a hyperfine splitting constant of $A_{iso}$=86G indicating only presence of $Mn^{2+}$ ions in anatase like coordination

-illumination of the sample with $Mn^{2+}$ ions within bulk core in anatase octahedral symmetry does not have any effect on the EPR signal for $Mn^{2+}$
-$Mn^{2+}$ ions does not participate in charge separation process

-high spin state of Mn (II) dopant

Magnetization curve for the spin coated Mn doped $TiO_2$ nanocrystalline thin film

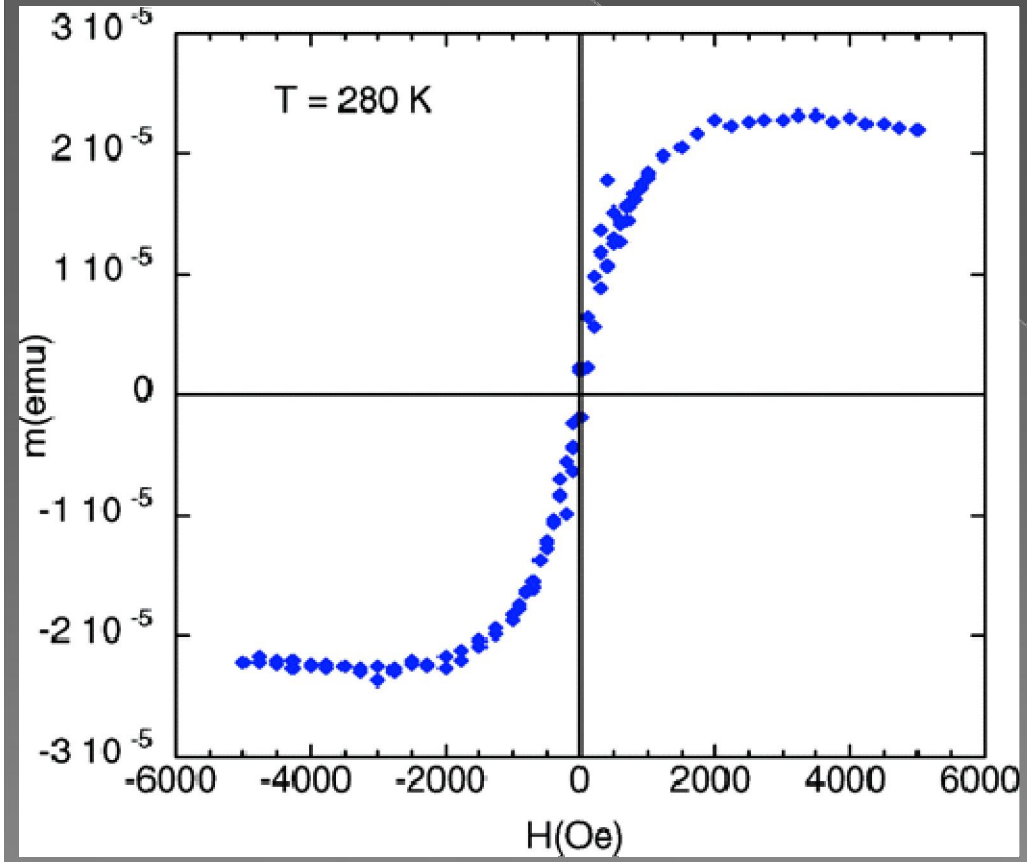


Saturation magnetic moment of $1.23\mu_B$

-exchange interaction between Mn atoms within nanoparticles

-absence of ordering of Mn atoms within anatase crystal structure

-absence of long-range ordering of nanocrystals in the film

Conclusions:

- hydrothermal synthesis of Mn doped $TiO_2$ anatase nanoparticles,

-$Mn^{2+}$ ions occupy two different sites having different binding energy,

-contribution to the paramagnetic behavior

-contribution in the light excitation process